Progress in Neurobiology 245 (2025) 102704

Contents lists available at ScienceDirect

Progress in Neurobiology

journal homepage: www.elsevier.com/locate/pneurobio

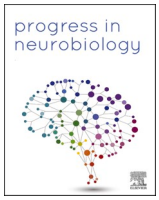

Cyto-, gene, and multireceptor architecture of the early postnatal mouse hippocampal complex

Ling Zhao [a,b,*,1], Menno P. Witter [c], Nicola Palomero-Gallagher [b,d]

[a] Department of Psychology, School of Public Policy and Management, Nanchang University, Nanchang 330000, China
[b] Institute of Neuroscience and Medicine (INM-1), Research Centre Jülich, Jülich 52425, Germany
[c] Kavli Institute for Systems Neuroscience, NTNU Norwegian University of Science and Technology, Trondheim, Norway
[d] C. & O. Vogt Institute for Brain Research, Heinrich-Heine-University, Dusseldorf 40225, Germany

ARTICLE INFO

Keywords:
Cytoarchitecture
Receptor architecture
Gene expression
Developing mouse brain
Postnatal day
Subicular complex

ABSTRACT

Neurotransmitter receptors are key molecules in signal transmission in the adult brain, and their precise spatial and temporal balance expressions also play a critical role in normal brain development. However, the specific balance expression of multiple receptors during hippocampal development is not well characterized. In this study, we used quantitative *in vivo* receptor autoradiography to measure the distributions and densities of 18 neurotransmitter receptor types in the mouse hippocampal complex at postnatal day 7, and compared them with the expressions of their corresponding encoding genes. We provide a novel and comprehensive characterization of the cyto-, gene, and multireceptor architecture of the developing mouse hippocampal and subicular regions during the developmental period, which typically differs from that in the adult brain. High-density receptor expressions with distinct regional and laminar distributions were observed for AMPA, Kainate, mGluR2/3, $GABA_A$, $GABA_A$/BZ, α_2, and A_1 receptors during this specific period, whereas NMDA, $GABA_B$, α_1, M_1, M_2, M_3, nicotinic $\alpha_4\beta_2$, 5-HT_{1A}, 5-HT_2, D_1 and D_2/D_3 receptors exhibited relatively low and homogeneous expressions. This specific balance of multiple receptors aligns with regional cytoarchitecture, neurotransmitter distributions, and gene expressions. Moreover, contrasting with previous findings, we detected a high α_2 receptor density, with distinct regional and laminar distribution patterns. A non-covariation differentiation phenomenon between α_2 receptor distributions and corresponding gene expressions is also demonstrated in this early developmental period. The multimodal data provides new insights into understanding the hippocampal development from the perspective of cell, gene, and multireceptor levels, and contributes important resources for further interdisciplinary analyses.

1. Introduction

The hippocampal complex constitutes a core element of the limbic system, and its proper development is indispensable to ensure normal functions of learning and memory, spatial navigation, emotion processing, and social behavior (Bird and Burgess, 2008; Dudek et al., 2016; Snyder et al., 2011; Zhong et al., 2020). The hippocampal complex consists of the hippocampus proper, which is subdivided into the dentate gyrus (DG) and the *Cornu Ammonis* (CA, with the CA3-CA1 regions), and the subicular complex, which contains the subiculum proper, presubiculum, parasubiculum, and postsubiculum (Fig. 1A). The DG region, the primary input gateway to the hippocampus, is more developmentally protracted than other cortical regions and its neurogenesis remains active across mouse lifespan (Cameron and McKay, 2001; Parisot et al., 2017; Snyder, 2019; Zhou et al., 2022). The CA3 region encompasses an unusual auto-associative memory network, and its abundant and intricate synaptic interconnections with the CA1 region provide a critical neuroanatomical substrate for short-term and long-term potentiation (Acsády and Káli, 2007; Ecker et al., 2022). The subiculum is, together with the CA1 region, the major information output structure of the hippocampal formation (van Strien et al., 2009; Zeineh et al., 2017), while the presubiculum and postsubiculum are key components of the head-direction system, which play critical roles in landmark navigation (Simonnet et al., 2017). Dysfunction of these

* Corresponding author at: Department of Psychology, School of Public Policy and Management, Nanchang University, Nanchang 330000, China.
E-mail address: lingzhao@ncu.edu.cn (L. Zhao).
[1] ORCID: 0000–0003-0902–1425

https://doi.org/10.1016/j.pneurobio.2024.102704
Received 13 October 2024; Received in revised form 27 November 2024; Accepted 13 December 2024
Available online 19 December 2024

hippocampal regions, which involves abnormal expression and activation of neurotransmitter receptors (Groc and Choquet, 2020; Lau and Zukin, 2007; Paoletti et al., 2013), is tightly associated with various neurological and psychiatric disorders, e.g., epilepsy and neurodevelopmental disorder autism spectrum disorder (Berger et al., 2020; Debski et al., 2020; Nagode et al., 2017; Represa et al., 1989).

Formation and development of proper anatomically and functionally distinct brain areas is crucial for normal brain function, including higher order cognitive functions and social behaviors (O'Leary et al., 2007, 2013; Xu et al., 2021). The developmental and differentiated mechanism of the cerebral cortex referred to as arealization are currently thought to involve an interplay between intrinsic genetic mechanisms, neurotransmitter receptor regulations, and extrinsic information inputs (Cameron et al., 1998; Crews et al., 2007; Herlenius and Lagercrantz, 2004; Levitt et al., 1997; O'Leary et al., 2007, 2013; Wang and Kriegstein, 2009; Xu et al., 2021). This process of cortical development is dynamic and follows precisely orchestrated processes which involve neurogenesis, neuronal migration, neuronal differentiation, synapse formation, as well as formation of intricate synaptic circuits (Chiang et al., 2021; Crews et al., 2007; Hippenmeyer, 2014; O'Leary et al., 2007, 2013; Wang and Kriegstein, 2009). Within this framework, postnatal day 7 (P7) is a critical period for mouse brain development, since projection neurons have finalized migration to the target lamina and cortical layers have just been established (Hippenmeyer, 2014). As key molecules of signaling transmission, the precise temporo-spatial expression and proper organization of neurotransmitter receptors is critical in the aforementioned brain developmental progress (Herlenius and Lagercrantz, 2004; Luján et al., 2005; Wang and Kriegstein, 2009). However, the role neurotransmitter receptors play in cortical development processes remains less well understood than that of transcription factors. Thus, the P7 mouse provides a vital window to study the multireceptor balance expressions during this cortical developing period.

Neurotransmitter receptors present specific regional and laminar expression patterns across brain (Palomero-Gallagher and Zilles, 2018; Zilles et al., 2002). Although positron emission tomography (PET) can be applied to quantify dynamic receptor changes *in vivo* brain, it is only accessible for a limited set of receptor types due to both technical and security restrictions, and has a relatively low resolution to clearly present the different regional and laminar receptor expression (Heiss and Herholz, 2006; Khan et al., 2021). Quantitative *in vitro* receptor autoradiography has been shown to be a powerful tool for visualization and quantification of multiple receptors in neighboring sections of the same brain and provides a high resolution able to capture differences in both regional and laminar receptor expressions (Palomero-Gallagher and Zilles, 2018; Zilles et al., 2002). Mouse models, especially transgenic mouse animals, have been shown to provide crucial insights and potentials in the field of disease and brain development (Feng et al., 2021; McGowan et al., 2006; Nagode et al., 2017; Witter, 2012; Xu et al., 2021). Although receptor expression patterns of adult mouse brain have been analyzed in previous studies (Cremer et al., 2011, 2015a, 2015b; Lothmann et al., 2021; Oermann et al., 2005; Vogt et al., 2013), the cyto- and multireceptor architectures of the mouse brain at the developmental P7 stage has not yet been systematically studied.

We here aimed to systematically dissect the cyto- and multireceptor architectures of mouse hippocampal complex at the developmental P7 stage, comparing with those found in adult brain. In addition, we also compared the distributions of multiple receptors in P7 mouse brain with their corresponding gene expressions (https://developingmouse.brain-map.org/). The regional and laminar receptor distributions of 18 different receptor types from 7 neurotransmitter systems were characterized by quantitative *in vitro* receptor autoradiography, and the multireceptor densities of each cytoarchitecturally identified area were projected to 3D mouse atlas and visualized as a receptor fingerprint to show the multireceptor balance expression. The present study sheds a new insight into understanding the mechanisms of brain development from the perspectives of both receptor and gene expressions, and provides a valuable data resource for future modelling and simulation studies.

2. Material and methods

2.1. Animals

Six male mouse brains were used for this multimodal cyto- and receptor architectonic analysis. All experimental mice (C57BL/6 J) were postnatal day 7 (P7) and kindly provided by Dr. Kevin Jones and Dr. Shen-Ju Chou. Animal care and experimental procedures were performed in accordance with guidelines of the Academia Sinica Institutional Animal Care and Use Committee. In addition, cytoarchitecture data from six male adult mice were obtained from the Research Center Jülich and exclusively used for conducting cytoarchitectonic comparative analysis with P7 mice. These adult mice were sourced from Helmholtz Center Munich, and the experimental protocols have been carried out in compliance with the guidelines of the European Communities Council Directive for the care and use of animals for scientific purposes.

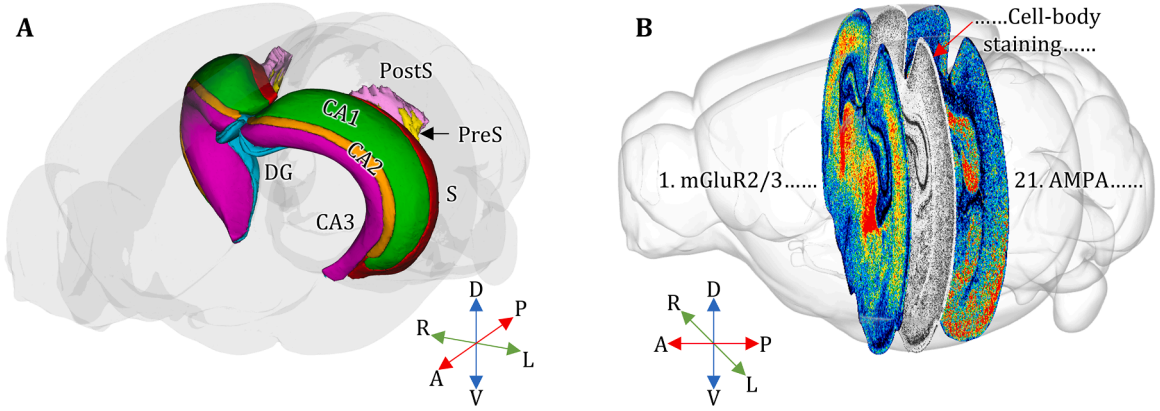

Fig. 1. 3D rendering of the mouse hippocampal complex and schematic representation of experimental setup. A) Regions of the hippocampal complex analyzed in the present study, each coded with specific color. The parasubiculum wasn't analyzed in the current study due to its caudal location in the mouse brain, the prosubiculum was not distinguishable from the subiculum, and the dorsal and ventral parts of the hippocampal complex were not separated at this early developmental period either (P7). B) Schematic representation of neighboring sections alternately destined to use for histological staining or visualization of 18 different receptor binding sites. Six brains were used for this multimodal cyto- and receptor architectonic analysis. Abbreviations: CA1-CA3, sectors 1–3 of the *Cornu Ammonis*; DG, dentate gyrus; PostS, postsubiculum; PreS, presubiculum; S, subiculum; A, anterior; P, posterior; D, dorsal; V, ventral; L, left; and R, right.

2.2. Tissue processing

The mice were sedated by CO_2 inhalation and subsequently decapitated. The brain was removed carefully from the skull without damaging its surface, especially when removing bone fragments. The meninges and blood vessels were not removed, since this process inevitably results in damaging of the pial surface and leads to a partial loss of cortical layer I. Each mouse brain was placed on a sheet of aluminum foil in a manner that preserved its normal shape, and slowly immersed in *N*-methylbutane (isopentane) under constant monitoring of temperature (kept between −40°C and −50°C) for approximately one minute. This method not only enables the brain tissue to be shock-frozen, but also avoids the appearance of freezing artifacts such as ice crystals, which would destroy the cellular morphology. The frozen brain was removed from the isopentane and placed in a pre-cooled plastic bag, which was left open in the freezer (-20°C) for about 10–15 minutes so that the excess isopentane could evaporate. The plastic bag was then sealed and stored in a freezer at −80°C until further processing.

2.3. Tissue sectioning

For each entire brain (without the cerebellum), it was serially sectioned along the anterior-posterior axis at around −15°C in the coronal plane using a cryostat microtome (Leica, Germany). Each section (10 μm thickness) was carefully thaw-mounted onto a pre-cooled, silanized glass slide and dried on a heating plate at 35°C to prevent the appearance of bubbles or folds. We acquired approximately 600 sections per brain, and the sections were organized into 21 groups or series. Therefore, each group contained about 29 sections, with ten sections spanning the hippocampal complex from anterior to posterior regions. The eleventh group from all six brains was processed for histological myelin staining, the sixth and sixteenth for cell-body staining, and the other eighteen for *in vitro* receptor autoradiography (Fig. 1B). For each receptor type, approximately 60 sections (10 sections per brain × 6 brains) were used for analyses of the hippocampal complex. Sections were stored in air-tight plastic bags at −80°C until further processing.

2.4. Histological staining and quantitative in vitro receptor autoradiography

The histological cresyl violet staining and a modified silver method (Gallyas, 1979) were performed to visualize the cyto- and myeloarchitecture of the mouse hippocampal complex, respectively. Quantitative *in vitro* receptor autoradiography was applied for the high-resolution visualization of the regional and laminar distribution patterns of 18 classical neurotransmitter receptor types: glutamate (AMPA, NMDA, kainate, and mGluR2/3), GABA ($GABA_A$, $GABA_A$/BZ, and $GABA_B$), acetylcholine (M_1, M_2, M_3, and nicotinic $\alpha_4\beta_2$), noradrenaline (α_1 and α_2), serotonin ($5\text{-}HT_{1A}$ and $5\text{-}HT_2$), dopamine (D_1 and D_2/D_3), and adenosine (A_1). This method has the advantage of providing a very high degree of sensitivity and enabling the quantification of receptor densities at the microcircuit level, though not at the single cell level (Palomero-Gallagher and Zilles, 2018). The receptor binding procedures were performed following previously published standard protocols (Palomero-Gallagher and Zilles, 2018; Zilles et al., 2002), which consist of three main steps: a preincubation, a main incubation, and a rinsing step (Table 1). For each targeted receptor type and in parallel with the main incubation to measure the total binding of each tritiated ligand, an additional section from each brain was incubated with the tritiated ligand and a non-labeled specific displacer. This additional step allowed the determination of the proportion of non-displaceable (i.e., non-specific) binding. Specific binding was calculated as the difference between total binding and non-specific binding. Since non-specific binding accounted for less than 5 % of the total binding, the latter was defined as specific binding in this study (Palomero-Gallagher and Zilles, 2018; Zilles et al., 2002). The radioactively labelled brain sections were co-exposed with plastic tritiated standards (with known and increasing concentrations of radioactivity) against β radiation-sensitive films (Carestream Kodak BioMax MR Film) for 9–15 weeks depending on the receptor type.

2.5. Image acquisition and processing

Histological sections were digitized to produce high-resolution images (1 μm in-plane resolution; 8 bit images) using a TISSUEscope Huron Scanner (Huron, Canada). Autoradiographs were digitized with the image acquisition and processing system Axiovision (Zeiss, Germany) connected to a CCD camera (Axiocam MRm, Zeiss, Germany) with an S-Orthoplanar 60-mm macro lens (Zeiss, Germany) corrected for geometric distortions, as well as in-house-developed Matlab (The MathWorks, Natrick, MA) scripts. The resulting images were saved as 8-bit gray value images with a 2.5 μm in-plane spatial resolution. Then, the gray value of each pixel in an autoradiographic image was first nonlinearly transformed into a corresponding concentration of radioactivity (*R*, cpm) by interpolation into the calibration curve computed with the gray values of the co-exposed plastic tritiated standards, and subsequently linearly transformed into an image in which each gray value (ranging from 0, black, to 255, white) codes for a given receptor density (fmol/mg protein) using Eq. (1).

$$C_b = \frac{R}{E \bullet B \bullet W_b \bullet S_a} \bullet \frac{K_D + L}{L} \quad (1)$$

E is the efficiency of the scintillation counter for quantification of radioactivity by liquid scintillation counting, B is a decay constant which represents the number of decays per unit of radioactivity and time (Ci/min), W_b is the mass of protein (constant; mg), S_a is the specific activity of the specific ligand (Ci/mmol), K_D is the equilibrium dissociation constant of the specific ligand (nM), and L is the free concentration of the specific ligand during incubation (nM).

To provide a high-contrast visualization of laminar and regional receptor distribution patterns, and to facilitate comparisons with neighboring cell-body-stained histological sections as well as between different receptor types, a pseudo color coding of receptor autoradiographs was carried out with a linear contrast enhancement while preserving the absolute linear scaling between gray values and receptor densities. For the optimized visualization of the receptor distribution patterns in the autoradiographs, the spectral arrangement of 11 colors to equally spaced density ranges was used.

2.6. Multimodal border definition and quantitative receptor density acquisition

Borders between adjacent brain regions in the hippocampal complex, were first delineated on the histologically processed sections according to cytoarchitectonic criteria based on previous cytoarchitectonic studies (Dong, 2008; Paxinos et al., 2020; van Strien et al., 2009; Witter, 2012). To further precisely identify and delineate the hippocampal subregions, the cytoarchitectonically identified borders were transferred to the neighboring color-coded autoradiographs, cross-validated and adjusted based on the differential laminar and regional distribution patterns of different receptor types. Finally, the receptor densities of hippocampal subregions were extracted from autoradiographic images by means of the in-house-developed software AnaRec. Hereby, we finally extracted a total of 6652 receptor-density data points. And, the mean receptor densities of hippocampal regions for each of the receptor types were projected onto the 3D atlas (Allen Mouse Brain) by using tool of MeshView (https://www.nesys.uio.no/MeshView/).

2.7. Comparison of receptor distribution and corresponding gene expression

Receptor expressions are regulated by their corresponding encoding

Table 1
Receptor binding protocols.

Transmitter	Receptor	Ligand (nM)	Property/ Exposure-time	Displacer	Incubation buffer	Pre-incubation	Main incubation	Final rinsing
Glutamate	AMPA	[^{3}H]-AMPA (10.0) (Perkin-Elmer, Germany)	Agonist (15 weeks)	Quisqualate (10 μM)	50 mM Tris-acetate (pH 7.2) [+ 100 mM KSCN] *	3 × 10 min, 4 °C	45 min, 4 °C	1) 4 × 4 sec, 4 °C 2) Acetone/ glutaraldehyde (950 ml + 50 ml), 2 × 2 sec, 22 °C
	NMDA	[^{3}H]-MK−801 (3.3) (Perkin-Elmer, Germany)	Antagonist (12 weeks)	(+)MK−801 (100 μM)	50 mM Tris-HCl (pH 7.2) + 50 μM Glutamate [+ 30 μM Glycine + 50 μM Spermidine]*	15 min, 4 °C	60 min, 22 °C	1) 2 × 5 min, 4 °C 2) Distilled water, 1 × 1 dip, 4 °C
	Kainate	[^{3}H]-Kainate (9.4) (Perkin-Elmer, Germany)	Agonist (12 weeks)	SYM 2081 (100 μM)	50 mM Tris-citrate (pH 7.1) [+ 10 mM Ca^{2+}-acetate]*	3 × 10 min, 4 °C	45 min, 4 °C	1) 3 × 4 sec, 4 °C 2) Acetone/ glutaraldehyde (950 ml + 50 ml), 2 × 2 sec, 22 °C
	mGluR2/ 3	[^{3}H]-LY 341,495 (1.0) (Sigma-Aldrich, Germany)	Antagonist (10 weeks)	L-Glutamate (1 mM)	10 mM Phosphate buffer (pH 7.6) [+ 100 mM KBr]*	2 × 5 min, 22 °C	60 min, 4 °C	1) 2 × 5 min, 4 °C 2) Distilled water, 1 × 1 dip, 4 °C
GABA	$GABA_A$	[^{3}H]-Muscimol (7.7) (Perkin-Elmer, Germany)	Agonist (12 weeks)	GABA (10 μM)	50 mM Tris-citrate (pH 7.0)	3 × 5 min, 4 °C	40 min, 4 °C	1) 3 × 3 sec, 4 °C 2) Distilled water, 1 × 1 dip, 4 °C
	$GABA_A$/ BZ	[^{3}H]-Flumazenil (1.0) (Perkin-Elmer, Germany)	Antagonist (9 weeks)	Clonazepam (2 μM)	170 mM Tris-HCl (pH 7.4)	15 min, 4 °C	60 min, 4 °C	1) 2 × 1 min, 4 °C 2) Distilled water, 1 × 1 dip, 4 °C
	$GABA_B$	[^{3}H]-CGP 54626 (2.0) (Biotrend, Germany)	Antagonist (10 weeks)	CGP 55845 (100 μM)	50 mM Tris-HCl (pH 7.2) + 2.5 mM $CaCl_2$ x 2 H_2O	3 × 5 min, 4 °C	60 min, 4 °C	1) 3 × 2 sec, 4 °C 2) Distilled water, 1 × 1 dip, 4 °C
Acetylcholine	M_1	[^{3}H]-Pirenzepine (10.0) (Perkin-Elmer, Germany)	Antagonist (12 weeks)	Pirenzepine dihydrochloride (2 μM)	Modified Krebs-Buffer (pH 7.4)	15 min, 4 °C	60 min, 4 °C	1) 2 × 1 min, 4 °C 2) Distilled water, 1 × 1 dip, 4 °C
	M_2	[^{3}H]-Oxotremorine-M (1.7) (Perkin-Elmer, Germany)	Agonist (15 weeks)	Carbachol (10 μM)	20 mM HEPES-Tris (pH 7.5) + 10 mM $MgCl_2$ x 6 H_2O	20 min, 22 °C	60 min, 22 °C	1) 2 × 2 min, 4 °C 2) Distilled water, 1 × 1 dip, 4 °C
	M_3	[^{3}H]−4-DAMP (1.0) (Perkin-Elmer, Germany)	Antagonist (9 weeks)	Atropine sulfate (10 μM)	50 mM Tris-HCl (pH 7.4) + 0.1 mM PMSF + 1 mM EDTA x 2 H_2O	15 min, 22 °C	45 min, 22 °C	1) 2 × 5 min, 4 °C 2) Distilled water, 1 × 1 dip, 4 °C
	Nicotinic $\alpha_4\beta_2$	[^{3}H]-Epibatidine (0.11) (Perkin-Elmer, Germany)	Agonist (15 weeks)	Nicotine Di-D-Tartrate (100 μM)	15 mM HEPES (pH 7.5) + 120 mM NaCl + 5.4 mM KCl + 0.8 mM $MgCl_2$ x 6 H_2O + 1.8 mM $CaCl_2$ x 2 H_2O	20 min, 22 °C	90 min, 22 °C	1) 1 × 5 min, 4 °C 2) Distilled water, 1 × 1 dip, 4 °C
Noradrenaline	α_1	[^{3}H]-Prazosin (0.09) (Perkin-Elmer, Germany)	Antagonist (15 weeks)	Phentolamine Mesylate (10 μM)	50 mM Na/K-phosphate buffer (pH 7.4)	15 min, 22 °C	60 min, 22 °C	1) 2 × 5 min, 4 °C 2) Distilled water, 1 × 1 dip, 4 °C
	α_2	[^{3}H]-RX 821002 (1.4) (Perkin-Elmer, Germany)	Antagonist (15 weeks)	Phentolamine Mesylate (10 μM)	50 mM Tris-HCl (pH 7.7) + 100 μM $MnCl_2$ x 4 H_2O	15 min, 22 °C	90 min, 22 °C	1) 1 × 5 min, 4 °C 2) Distilled water, 1 × 1 dip, 4 °C
Serotonin	$5\text{-}HT_{1A}$	[^{3}H]−8-OH-DPAT (0.3) (Perkin-Elmer, Germany)	Agonist (15 weeks)	5-Hydroxy-Tryptamine (1 μM)	170 mM Tris-HCl (pH 7.7) [+ 4 mM $CaCl_2$ x 2 H_2O + 0.01 % Ascorbate]*	30 min, 22 °C	60 min, 22 °C	1) 1 × 5 min, 4 °C 2) Distilled water, 3 × 1 dips, 4 °C
	$5\text{-}HT_2$	[^{3}H]-Ketanserin (1.14) (Perkin-Elmer, Germany)	Antagonist (15 weeks)	Mianserin HCl (10 μM)	170 mM Tris-HCl (pH 7.7)	30 min, 22 °C	120 min, 22 °C	1) 2 × 10 min, 4 °C 2) Distilled water, 3 × 1 dips, 4 °C
Dopamine	D_1	[^{3}H]-SCH 23390 (1.67) (Perkin-Elmer, Germany)	Antagonist (15 weeks)	SKF 83566 (1 μM)	50 mM Tris-HCl (pH 7.4) + 120 mM NaCl + 5 mM KCl + 2 mM $CaCl_2$ x 2 H_2O + 1 mM $MgCl_2$ x 6 H_2O	20 min, 22 °C	90 min, 22 °C	1) 2 × 10 min, 4 °C 2) Distilled water, 1 × 1 dip, 4 °C

(*continued on next page*)

Table 1 (*continued*)

Transmitter	Receptor	Ligand (nM)	Property/ Exposure-time	Displacer	Incubation buffer	Pre-incubation	Main incubation	Final rinsing
					[+ 1 μM Mianserin] *			
	D_2/D_3	[^{3}H]-Fallypride (4.0) (Institute for Nuclear Chemistry, University of Mainz, Germany)	Antagonist (15 weeks)	Haloperidol (10 μM)	50 mM Tris-HCl (pH 7.4) + 120 mM NaCl + 5 mM KCl	30 min, 22 °C	60 min, 37 °C	1) 2 × 2 min, 4 °C 2) Distilled water, 1 × 1 dip, 4 °C
Adenosine	A_1	[^{3}H]-DPCPX+Gpp(NH)p (0.75) (Perkin-Elmer, Germany)	Agonist (10 weeks)	R-PIA (100 μM)	170 mM Tris-HCl (pH 7.4) + 2 Units/l Adenosine deaminase [+ 100 μM Gpp (NH)p]*	15 min, 4 °C	120 min, 22 °C	1) 2 × 5 min, 4 °C 2) Distilled water, 1 × 1 dip, 4 °C

* only included in the main incubation. The agonistic ligands of [^{3}H]-Muscimol label the orthosteric binding site of $GABA_A$ at the interface of the α and β subunits, including the receptor subtypes containing the δ subunit which are typically found in extrasynaptic or perisynaptic regions. In contrast, the antagonistic ligands of [^{3}H]-Flumazenil label the allosteric binding site for benzodiazepines on $GABA_A$ ($GABA_A$/BZ), located at the junction of an α (α_1, α_2, α_3 or α_5) and a γ_2 subunit (Chandra et al., 2010; Verdurand et al., 2013).

genes, however, the relationships between gene expression levels and neurotransmitter receptor densities remains elusive (Zhao et al., 2023). To analyze the developmental mechanisms at both the receptor and gene levels, we compared multireceptor distributions in the P7 mouse hippocampal complex with the corresponding gene expressions obtained from the Allen Developing Mouse Brain Atlas (https://developingmouse.brain-map.org/). We selected the gene data provided for P4 animals, as it was the closest available developmental stage in the dataset. Notably, the receptor data were obtained from coronal slices, whereas the sections used for gene expression analysis were obtained in the sagittal plane. The receptors and their corresponding encoding genes are specified in Zhao et al. (2023). In the case of ionotropic receptors, which are encoded by multiple subunit genes, we selected the main subunits based on previous studies (Borges et al., 2003; Chuang and Reddy, 2018; Luján et al., 2005) for analysis.

2.8. Comparison of receptor densities between P7 and adult mouse brains

To compare the different receptor expressions between the P7 and adult mouse brains, the mean densities of the analyzed 16 receptor types in the adult hippocampus were obtained using data from previous studies (Cremer et al., 2015a, 2015b; Lothmann et al., 2021; Oermann et al., 2005; Zilles et al., 2000). A Spearman correlation across multiple receptors was performed to study their relationships. Subsequently, a nonlinear Granger causality analysis was conducted using the mutual information approach (Kraskov et al., 2004).

2.9. Statistical analyses

To control for the drawbacks of experimental designs involving repeated measures due to the non-independent nature of the data to be analyzed, linear mixed-effects models (Baayen et al., 2008) were used to detect significant differences in receptor densities between adjacent regions. The most important strength of linear mixed-effects models is that they allow to simultaneously consider all fixed factors and random factors that potentially contribute to the understanding of the structure of the data. The models were conducted with the lmerTest package (Kuznetsova et al., 2017), which is based on the statistical programming environment R (version: 4.0.4) (https://www.r-project.org/).

The linear mixed model was first constructed and then refined by defining hippocampal area and receptor type as fixed factors, while subject (mouse brain) was set as a random factor (Eq. (2) (Barr et al., 2013; Bates et al., 2015). After running the refined model, the statistical results of an omnibus test were obtained which consisted of main effects of hippocampal area and receptor type, the interaction effect between hippocampal area and receptor type, the fixed effects of hippocampal area and receptor type, as well as the random effects of subject which included the random intercept. As the interaction effect between hippocampal area and receptor type was found to be significant ($p < 0.001$), the simple effect of hippocampal area for each receptor type (i.e., 18 simple effects) was analyzed to determine whether there was a significant difference of receptor density across all hippocampal subareas for each receptor type (*F* test, Table 2). Then, post hoc analyses were performed for each receptor separately to determine the significant differences in receptor densities between adjacent brain regions (*t* test, Table 3). The false discovery rate (FDR) approach (Benjamini and Hochberg, 1995) was used for multiple comparisons in simple effect and post hoc analyses, respectively.

$$RD_{arb} = \alpha_0 + \alpha_1 A_a + \alpha_2 R_r + \alpha_3 A_a R_r + \alpha_4 B_b \quad (2)$$

where RD is the receptor density, A is hippocampal area, R is receptor type, and B is mouse brain.

In addition, the percentage width of the stratum pyramidale (SP) relative to the cortical thickness of the CA1 region were measured from each of 6 P7 and adult brains, respectively. And, a non-parameter permutation test (Nichols and Holmes, 2002) was performed to test their significant difference.

2.10. Multivariate analyses of receptor fingerprints

Multireceptor expressions in a single architectonically defined brain region has been visualized as a receptor fingerprint (Geyer et al., 1998; Zilles et al., 2002), which is a polar-coordinate plot simultaneously showing the mean densities of multiple receptor types in a given brain region. This region-specific balance of multireceptor expressions reveals the locally specific neurochemical organization at the receptor level. In addation, principal component (PCA), hierarchical cluster (HCA), and *k*-means analyses were carried out separately for multireceptor densities to determine the grouping of different hippocampal regions based on differences in the size and shape of their fingerprints. The Euclidean distance and Ward linkage algorithm were used to calculate the similarities between receptor fingerprints in the HCA. Subsequent, the number of stabile clusters was defined by the *k*-means analysis combining elbow method (Rousseeuw, 1987).

Table 2
Mean receptor densities (in fmol/mg protein; ± standard deviation) of mouse hippocampal complex at P7 developmental period.

Type	Receptor density ($n = 6$)							p-value
	DG	CA3	CA2	CA1	S	PreS	PostS	
AMPA	905 ± 106	1898 ± 208	1627 ± 151	1407 ± 211	1414 ± 162	874 ± 95	752 ± 107	<0.001*
NMDA	380 ± 42	456 ± 53	472 ± 64	469 ± 56	459 ± 45	397 ± 63	390 ± 48	<0.001*
Kainate	880 ± 107	841 ± 78	770 ± 85	796 ± 76	1565 ± 162	1305 ± 187	1164 ± 129	<0.001*
mGluR2/3	2665 ± 259	2342 ± 199	2985 ± 324	3968 ± 564	5903 ± 579	5820 ± 862	7087 ± 654	<0.001*
$GABA_A$	1093 ± 163	1412 ± 178	1683 ± 190	1705 ± 223	2316 ± 247	2542 ± 316	2640 ± 278	<0.001*
$GABA_A$/BZ	1142 ± 188	1967 ± 347	2068 ± 417	2023 ± 340	2608 ± 368	2414 ± 341	2423 ± 322	<0.001*
$GABA_B$	535 ± 94	666 ± 155	559 ± 127	485 ± 99	559 ± 105	593 ± 135	567 ± 141	<0.001*
M_1	341 ± 67	443 ± 79	440 ± 72	449 ± 73	401 ± 62	373 ± 68	422 ± 80	<0.001*
M_2	80 ± 23	107 ± 30	108 ± 29	87 ± 26	99 ± 31	103 ± 35	145 ± 51	<0.001*
M_3	270 ± 45	314 ± 52	343 ± 60	354 ± 59	349 ± 69	286 ± 54	285 ± 67	<0.001*
$\alpha_4\beta_2$	148 ± 23	150 ± 22	150 ± 26	163 ± 26	232 ± 34	385 ± 50	364 ± 26	<0.001*
α_1	66 ± 12	75 ± 12	76 ± 15	69 ± 14	87 ± 12	74 ± 13	74 ± 13	<0.001*
α_2	360 ± 31	308 ± 21	348 ± 26	658 ± 89	859 ± 123	467 ± 66	344 ± 59	<0.001*
5-HT_{1A}	40 ± 10	43 ± 10	49 ± 13	48 ± 15	36 ± 9	68 ± 18	76 ± 23	<0.001*
5-HT_2	95 ± 16	103 ± 16	103 ± 17	96 ± 15	99 ± 16	99 ± 16	98 ± 16	0.109
D_1	92 ± 17	154 ± 24	171 ± 36	110 ± 17	131 ± 22	98 ± 17	99 ± 20	<0.001*
D_2/D_3	90 ± 9	90 ± 8	89 ± 11	93 ± 9	100 ± 8	89 ± 15	83 ± 12	<0.001*
A_1	419 ± 106	796 ± 219	847 ± 250	748 ± 201	886 ± 238	761 ± 211	777 ± 228	<0.001*

Six mouse brains were used to extract mean receptor densities of the hippocampal complex at the P7 developmental period. Nominal p-values resulting from the analysis of the simple effect of hippocampal area for each receptor type underwent FDR correction (*).

Table 3
Results of post hoc tests present the differences in densities of each receptor between adjacent hippocampal regions.

Receptor	Post hoc tests						
	DG vs CA3	CA3 vs CA2	CA2 vs CA1	CA1 vs S	S vs PreS	S vs PostS	PreS vs PostS
AMPA	<0.001*	<0.001*	<0.001*	0.655	<0.001*	<0.001*	0.080
NMDA	<0.001*	0.299	0.825	0.502	<0.001*	<0.001*	0.972
Kainate	0.309	0.067	0.425	<0.001*	<0.001*	<0.001*	0.003
mGluR2/3	0.027	<0.001*	<0.001*	<0.001*	0.386	<0.001*	<0.001*
$GABA_A$	<0.001*	<0.001*	0.729	<0.001*	0.002	<0.001*	0.347
$GABA_A$/BZ	<0.001*	0.170	0.530	<0.001*	0.016	0.011	0.995
$GABA_B$	<0.001*	<0.001*	<0.001*	0.001*	0.218	0.798	0.380
M_1	<0.001*	0.844	0.586	0.001*	0.128	0.317	0.026
M_2	<0.001*	0.783	<0.001*	<0.001*	0.582	<0.001*	<0.001*
M_3	<0.001*	0.013	0.260	0.558	<0.001*	<0.001*	0.720
$\alpha_4\beta_2$	0.790	0.943	0.067	<0.001*	<0.001*	<0.001*	0.035
α_1	0.001*	0.495	0.007	<0.001*	<0.001*	<0.001*	0.721
α_2	0.002	0.021	<0.001*	<0.001*	<0.001*	<0.001*	<0.001*
5-HT_{1A}	0.073	<0.001*	0.337	<0.001*	<0.001*	<0.001*	0.001*
5-HT_2	0.024	0.909	0.036	0.463	0.384	0.867	0.523
D_1	<0.001*	<0.001*	<0.001*	<0.001*	<0.001*	<0.001*	0.960
D_2/D_3	0.889	0.714	0.120	0.021	0.006*	<0.001*	0.126
A_1	<0.001*	0.023	<0.001*	<0.001*	<0.001*	<0.001*	0.778

Nominal p-values resulting from the analysis of the post hoc tests of hippocampal area for each receptor type underwent FDR correction (*).

3. Results

3.1. Cytoarchitecture of the hippocampal regions in P7 and adult brains

3.1.1. Dentate gyrus

The dentate gyrus encompasses the CA4 region of the *Cornu Ammonis* and the fascia dentata (FD), which consists of three layers (Fig. 2). The outer layer or stratum moleculare (SM) of the FD, found partly on the free surface and partly separated from the *Cornu Ammonis* and subiculum by the hippocampal fissure, is a relatively cell free layer in the adult brain, but at P7 it presents a slightly higher number of scattered neuronal cell bodies. The stratum granulosum (SG) or principal cell layer of the FD, located deeper with respect to SM, is characterized by many granular cell bodies. However, these granule cells are less densely packed in the P7 than in the adult mouse brain (Fig. 2), and the SG appears broader and not well-defined in the P7 mouse brain. The third layer of the FD, the polymorphic layer (PML), is enclosed by the SG and SM, which form a convoluted "V" or "U" shaped region around the CA4 region. The PML appears to have a higher cellular density in the P7 than in the adult mouse brain. Together with the CA4 region, it constitutes the hilus.

3.1.2. Cornu Ammonis

Differences in packing density of the principal cell type of the CA region enable differentiation of the CA3, CA2, and CA1 regions. They present a generally similar three-layered laminar organization consisting of two molecular layers separated by a cellular layer which contains the cell bodies of the main cellular type in the CA region, i.e., the pyramidal cells (Fig. 2):

- The most superficial layer, bordering the hippocampal fissure or the free pia surface of the hemisphere, is the outer molecular layer composing of two sublayers: the stratum lacunosum-moleculare (SLM) and the stratum radiatum (SR), which contain the distal and proximal portions of the pyramidal cell's dendritic tree, respectively. Additionally, the CA3 region presents a stratum lucidum (SL), a narrow acellular interlayer which comprises the mossy fiber axons originating from the DG. The architectonically classical criterion of identifying the CA3/CA2 border, the mossy fibers are most noted for bending ventrally to form an "end bulb" at the distal end of the SL, is

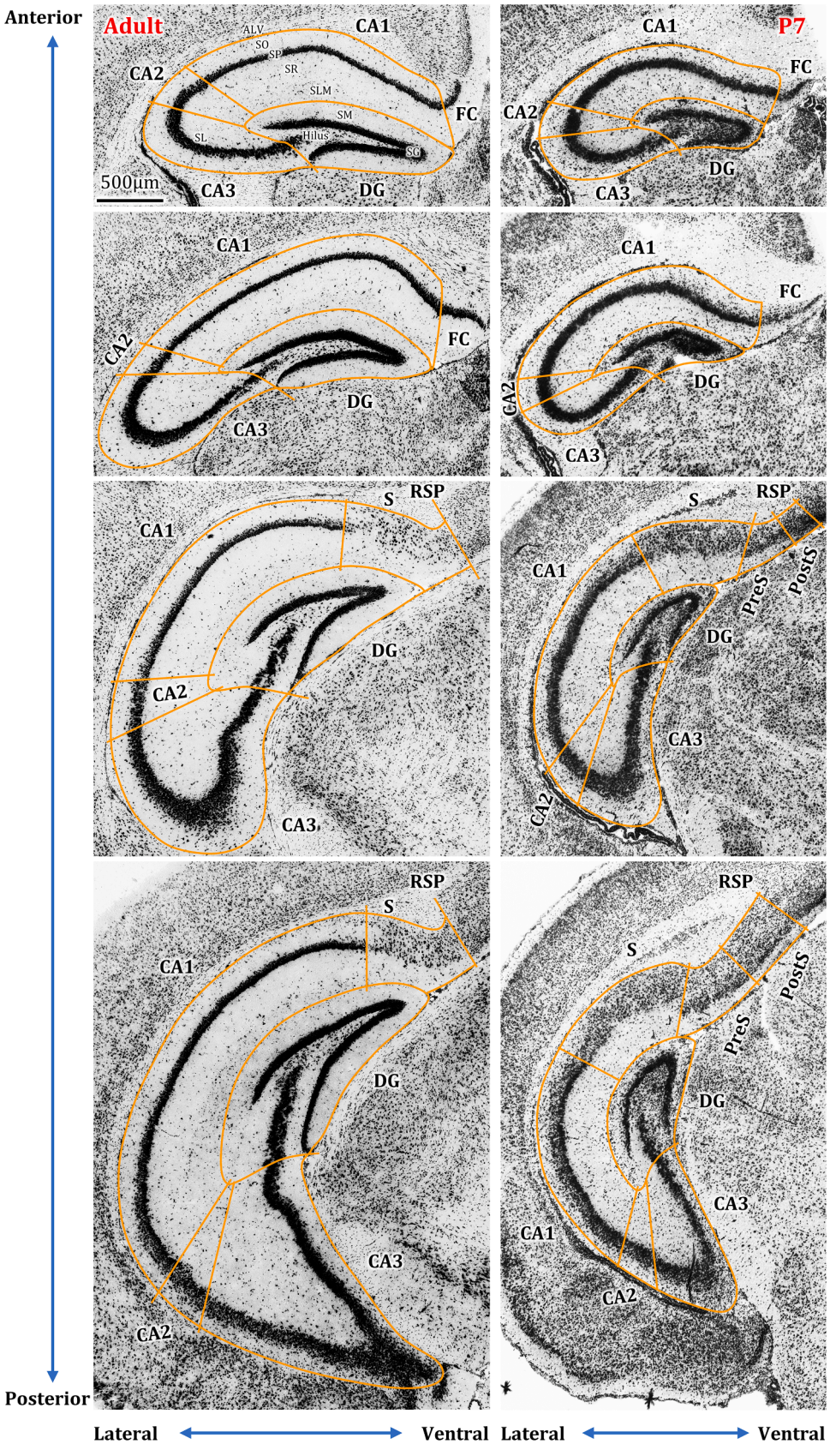

(caption on next page)

Fig. 2. Coronal sections (10 μm thickness) stained by cresyl violet for cell bodies and showing the regional and laminar cytoarchitecture of the hippocampus complex in adult and P7 mouse brains. The histologic sections from six adult mice were obtained from previous studies performed at the Research Center Jülich. The width of SP relative to the entire width of the CA1 region was measured in P7 and adult mouse brain using the high resolution digitized histological images throughout all rostro-caudal levels. Subsequently, a non-parametric permutation test (Nichols and Holmes, 2002) revealed that the SP is significantly wider in P7 compared to adult brains (12 % and 6 % of the total width of the CA1 region in P7 and adult brains, respectively, $p < 0.001$; Supplementary Fig. S1). Abbreviations: CA1-CA3, sectors 1–3 of *Cornu Ammonis*; DG, dentate gyrus; FC, fasciola cinereum; ALV, alveus; SG, stratum granulosum; SL, stratum lucidum; SLM, stratum lacunosum-moleculare; SM, stratum moleculare; SO, stratum oriens; SP, stratum pyramidale; SR, stratum radiatum; S, subiculum; PreS, presubiculum; PostS, postsubiculum; and RSP, retrosplenial cortex.

not as clearly visible in the P7 as in the adult mouse brain. Furthermore, the outer molecular layers of the P7 mouse brain contain relatively more scattered neuronal cell bodies than their counterparts in the adult mouse brain.

- The cellular layer, the stratum pyramidale (SP), is populated by pyramidal cell bodies with varying sizes and degrees of packing density. In both age groups, the pyramidal neurons in CA3 and CA2 are relatively larger and less densely packed than the pyramidal neurons of CA1. However, the overall pyramidal cell packing density in the P7 mouse brain is relatively lower than in the adult brain, and the width of the SP relative to the total cortical thickness of the CA1 region is significantly larger in the P7 than in the adult stage (12 % and 6 % in P7 and adult brains, respectively, $p < 0.001$; Supplementary Fig. S1).
- The deepest layer of the hippocampus, the so-called inner molecular layer, is occupied solely by the narrow, relatively cell-free stratum oriens (SO). Comparable to the situation described for the outer molecular layers, the SO of P7 mice presents relatively more scattered neuronal cell bodies than that of adult mice. The fiber-containing alveus (ALV; the white matter of the hippocampus) is immediately below the SO.

3.1.3. Subicular complex

The subicular complex encompasses the subiculum (S), presubiculum (PreS) and postsubiculum (PostS) in the present study, and presents the typical cytoarchitectonic characteristics of allocortex, i.e., three layers. The S is characterized by a broad pyramidal cell layer which is clearly distinguishable from the considerably narrower SP in the neighboring CA1. In addition, the SO and SLM of CA are no longer present in the S. Furthermore, the molecular layer of S is subdivided into superficial and deeper portions that are continuous with the SLM and SR of CA1, respectively (Figs. 2 and 3). Interestingly, the pyramidal cell packing density is relatively higher in the P7 mouse brain than in the adult brain, and the area of cellular layer is relatively boarder in the P7 than in the adult stage.

The PreS and PostS can be distinguished from the S by the disappearance of the deeper portion of the molecular layer and by changes in the cellular layer. In the S, this cellular layer is characterized by broadly and homogeneously distributed medium-sized pyramidal cells, whereas in the PreS and PostS it is composed of many small pyramidal cells and subdivided into a densely packed second cellular layer which is located just below the relatively cell free molecular layer, and a somewhat more loosely packed third layer (Fig. 3). The pyramidal cells of the second layer are relatively more densely packed in PreS than in PostS, while in the third layer they are more loosely packed in the PreS than in the PostS. In addition, the PreS has a shallow cell-free strip between the second and third layers (the lamina dissecans), which is not clearly present in the PostS. Comparing with the adult mouse brain, the PreS and PostS are relatively appeared more rostrally in the P7 mouse brain (Fig. 2).

3.2. Receptor architecture of the P7 hippocampal regions

The regional and laminar distribution patterns of receptors for seven classical neurotransmitters are visualized by the receptor autoradiographs depicted in Figs. 3 and 4, and compared with the expressions of corresponding encoding genes (Fig. 5). Additionally, the specific regional and laminar distribution of each receptor type was consistently examined in all the analyzed brains. Furthermore, differences in mean receptor densities averaged from six brains between adjacent hippocampal subregions were analyzed for each of the 18 different receptor types (Tables 2 and 3). Subsequently, the mean receptor densities of hippocampal regions for each of the receptor types were projected onto the corresponding 3D hippocampal atlas (Fig. 6).

3.2.1. Glutamate receptors

3.2.1.1. AMPA receptor. The P7 mouse hippocampal regions show a distinct regional and laminar distribution pattern of AMPA receptors (Fig. 3). Mean AMPA receptor densities in the DG are significantly lower than in the CA region (Table 3). Densities decrease significantly when moving from the CA3 through CA2 to CA1 and then further between the S and the PreS and PostS, which present comparable densities. Interestingly, the corresponding encoding genes, *Gria1* and *Gria2*, exhibit similar expression patterns with relatively lower levels in the DG, PreS, and PostS than in the CA regions (Fig. 5). Within the DG region, the hilus presents a higher AMPA density than the molecular layer of FD. The AMPA receptors in the CA3 and CA2 regions show a relatively homogeneous and high-density distribution, while in the CA1 the receptor density is lower in the SR than in the SP or SLM. Within the subicular complex, the superficial layer of S displays a lower AMPA receptor density than does the deeper layer, and the opposite holds true for the PreS and PostS.

3.2.1.2. NMDA receptor. In general terms the NMDA receptors show a low density and relatively homogeneous distribution pattern in the P7 mouse hippocampal regions (Fig. 3). Conversely, the encoding genes *Grin1* and *Grin2b* present high expression levels and distinct regional and laminal patterns at P4 (Fig. 5). The DG presents a significantly lower receptor density than its neighboring region (Table 3). In addition, the receptor density of S is significantly higher than that of the PreS and PostS.

3.2.1.3. Kainate receptor. Kainate receptors are heterogeneously distributed throughout the P7 mouse hippocampal regions (Fig. 3). Of particular interest is the fact that the kainate receptor is the only one for which the DG region presents a higher density than the abutting CA region. Within the DG region, the SM and PML contain a higher receptor density than the SG. The CA region is characterized by a particularly low receptor density in the SP, which starts at the hilus/CA3 border and abruptly stops at the CA1/S border. The SL of CA3 displays a high receptor density and abruptly stops at the CA3/CA2 border. Within the subicular complex, kainate densities decrease significantly from the S through PreS to PostS (Table 3). Whereas the S shows a homogeneous receptor distribution pattern, and within the PreS and PostS the second layer presents a lower receptor density than the other two layers. Not coincidentally, similar expression patterns are also discovered in their encoding genes, especially in the subicular complex, where high expression levels are observed (Fig. 5).

3.2.1.4. mGluR2/3 receptor. A distinct regional and laminar distribution pattern of mGluR2/3 receptors can also be demonstrated in the P7 mouse hippocampal regions (Fig. 3). mGluR2/3 densities decrease

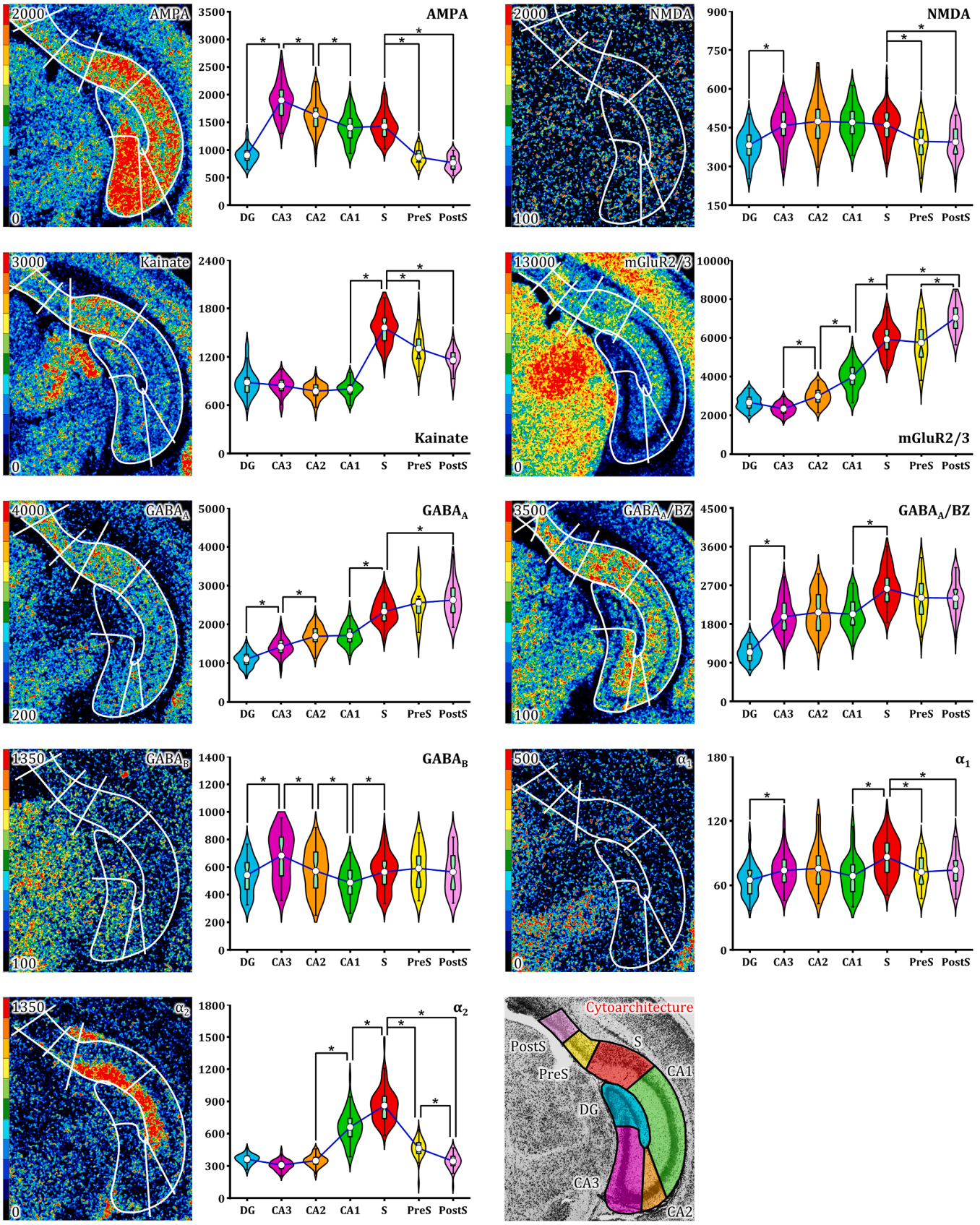

Fig. 3. The regional and laminar cyto- and receptor architecture of glutamate, GABA, and noradrenaline receptors in the P7 mouse hippocampal regions. The violin figures, representing mean receptor densities and distributions of individual section values from each of the six brains, show the different receptor-density expressions between the P7 hippocampal regions. The underlying data are provided in Tables 2 and 3. Asterisks indicate significant differences in receptor densities between neighboring regions after FDR correction. Abbreviations: CA1-CA3, sectors 1–3 of the *Cornu Ammonis*; DG, dentate gyrus; PostS, postsubiculum; PreS, presubiculum; and S, subiculum.

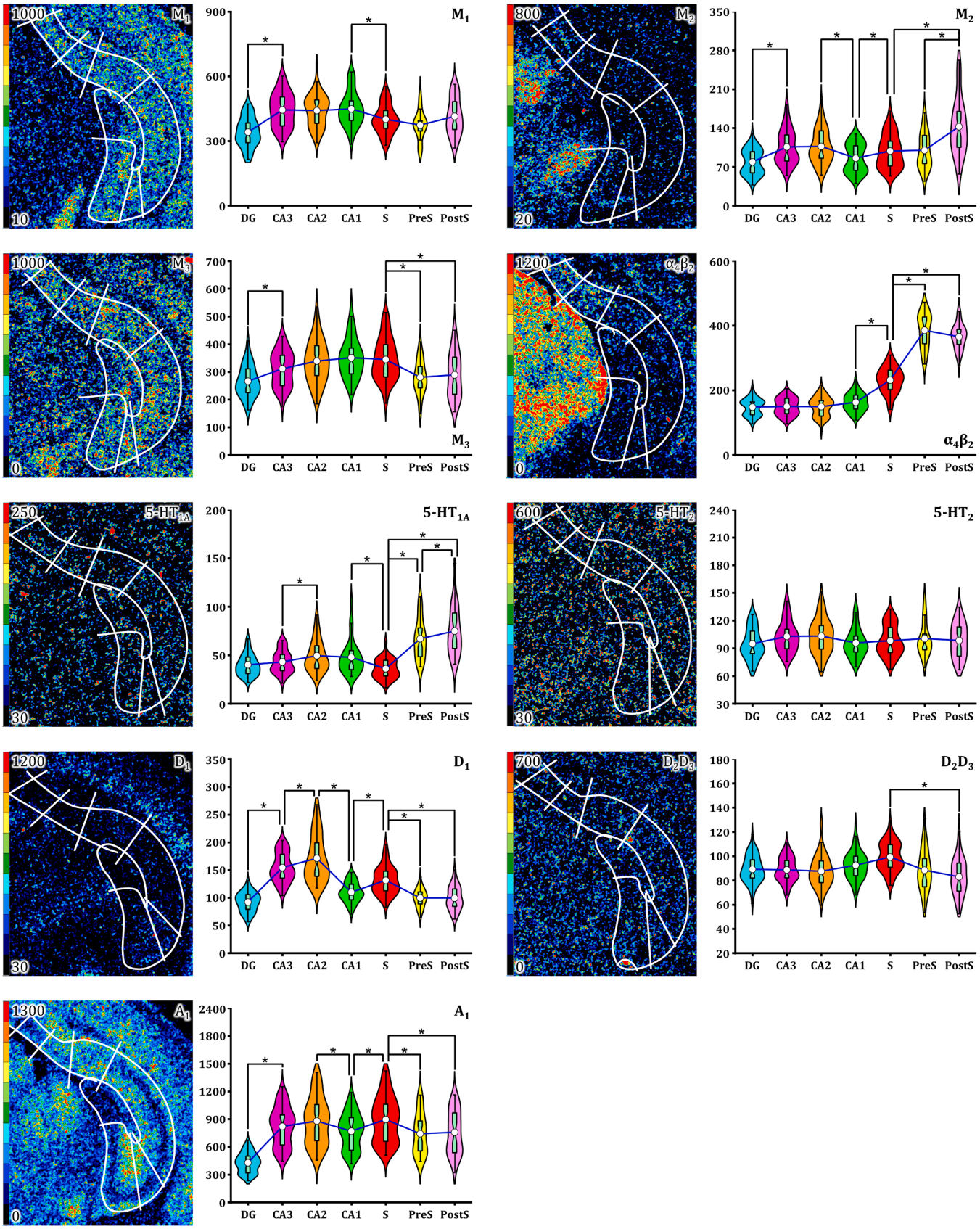

Fig. 4. The regional and laminar cyto- and receptor architecture of acetylcholine, serotonin, dopamine, and adenosine receptors in the P7 mouse hippocampal regions. The violin figures, representing mean receptor densities and distributions of individual section values from each of the six brains, show the different receptor-density expressions between the P7 hippocampal regions. The underlying data are provided in Tables 2 and 3. Asterisks indicate significant differences in receptor densities between neighboring regions after FDR correction. Abbreviations: CA1-CA3, sectors 1–3 of the *Cornu Ammonis*; DG, dentate gyrus; PostS, postsubiculum; PreS, presubiculum; and S, subiculum.

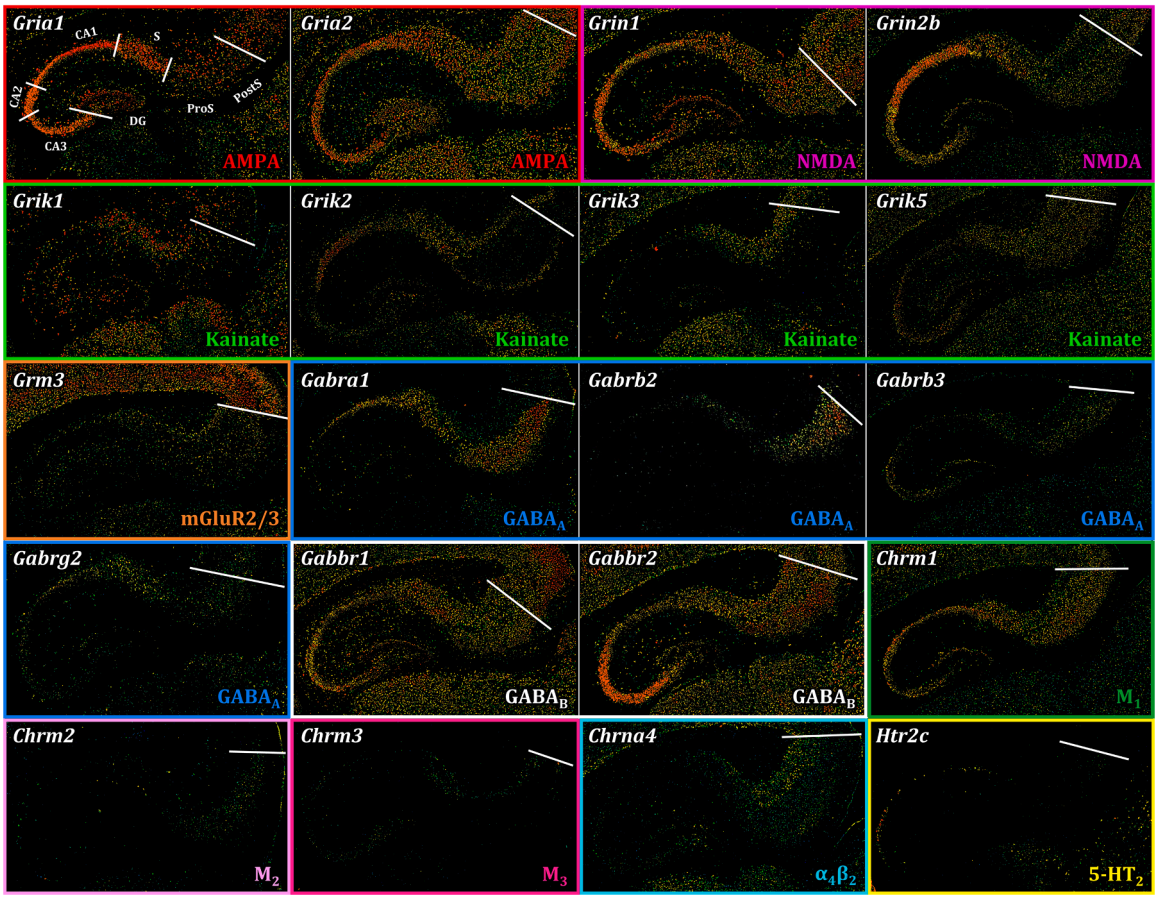

Fig. 5. Gene expressions of main receptor subunits in P4 mouse hippocampal complex. The gene expression data were obtained from the Allen Developing Mouse Brain Atlas (https://developingmouse.brain-map.org/). The genes encoding α_1 and A_1 receptors were not measured in this dataset and, therefore, are not shown in this study. Additionally, genes with extremely low expression levels are also not depicted, such as *Gria3*, *Grin2a*, *Grm2*, *Gabra2*, *Gabra3*, *Chrnb2*, *Htr1a*, *Drd1–3*, and *Adra2a-c*. See Supplementary Table S1 for the comprehensive list of receptors and encoding genes. Note, that our receptor data was obtained from coronal slices (see the different rostro-caudal levels depicted in the images shown in Figs. 3 and 4), and that sections used for gene expression analysis (a subset of which is presented in this figure) were obtained in the sagittal plane. Both of them were derived from the ventral hippocampal complex.

significantly from the S through the CA1, CA2 to CA3 (Table 3), and this is especially obvious in SLM. Thus, the CA2 can be distinguished from CA3 and CA1 by its significantly higher and lower receptor density in SLM, respectively. Furthermore, the SP of the CA region is visible as a clear low-density strip, which starts at the border with hilus and abruptly ends at the border between the CA1 and S. In the subicular complex, the PostS shows the highest-density receptor distribution, significantly higher than that in the S and PreS. At P4, relative to other developmental periods, the encoding genes *Grm2* and *Grm3* display relatively low and high expression levels, respectively (Fig. 5). This is particularly true for *Grm3* in the subicular complex.

3.2.2. *GABA receptors*

3.2.2.1. GABA$_A$. The GABA$_A$ receptor presents a regional heterogeneous distribution pattern in the P7 mouse hippocampus (Fig. 3). The mean receptor density is significantly lower in the DG than in its neighboring CA region (Table 3). In addition, the CA2 region contains significantly higher receptor density than the CA3 region. A homogeneously distributed and high-density receptor pattern in the subiculum enables its segregation from the PreS. Moreover, the S has a significantly higher receptor density than the CA1, while presents a significantly lower density than the PostS.

3.2.2.2. GABA$_A$/BZ. The P7 mouse hippocampal complex presents a distinct regional and laminar distribution pattern of GABA$_A$/BZ binding sites (Fig. 3). The lowest binding site density was measured in the DG region, which can be clearly distinguished from neighboring regions with their significantly higher densities (Table 3). Furthermore, compared with other layers within the CA region, the SP is highlighted as a low-density strip, which starts at the hilus/CA3 border and abruptly ends at the border between CA1 and S. Within the subicular complex, the S presents a homogeneous and high-density binding site distribution which can be distinctively distinguished from its adjacent regions with their significantly lower density, as well as from the PreS with its relatively lower density. In addition, the border between the PreS and PostS is clearly identified mainly by the PostS showing a higher binding site density in the second layer. Furthermore, the shared encoding genes of GABA$_A$ and GABA$_A$/BZ present comparable expression patterns, with decreasing levels from the subicular complex through the CA to DG (Fig. 5).

3.2.2.3. GABA$_B$. The GABA$_B$ receptor is present at a relatively low-density in the P7 mouse hippocampal regions (Fig. 3). Within the CA region, receptor densities decrease significantly when moving from the CA3 through CA2 to CA1, which also shows a significantly lower density than the S (Table 3). In addition, the CA3 presents a significantly higher density than the DG. Consistently, the encoding genes *Gabbr1* and *Gabbr2* exhibit distinct high expression levels in the CA3 and CA2 regions (Fig. 5).

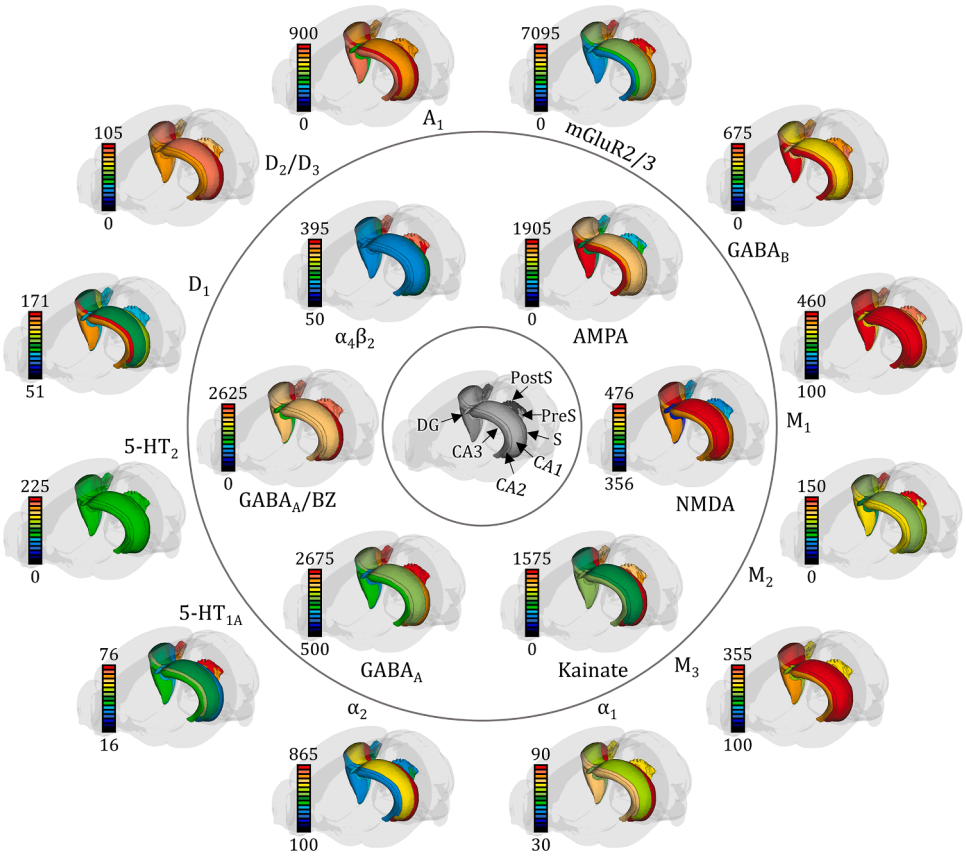

Fig. 6. 3D visualization of mean receptor densities of the P7 mouse hippocampal regions for each of the 18 different receptor types. It is worth noting that we used the same color bar for all receptor types; however, the same color corresponds to different receptor densities for each receptor type. Color bar codes for receptor densities in fmol/mg protein and the exact receptor densities of hippocampal regions for each receptor type are presented in Table 2, Figs. 3 and 4. Ionotropic receptors are organized within the inner circle, while metabotropic receptors are placed along the outer circle. Region labels are provided in the 3D maps of the mGluR2/3 receptors. (For interpretation of the references to color in this figure legend, the reader is referred to the web version of this article.)

3.2.3. *Noradrenaline receptors*

3.2.3.1. α_1. The α_1 receptors are present at an overall low-density in the P7 mouse hippocampal regions (Fig. 3). The DG presents a significantly lower receptor density than its abutting region the CA3 (Table 3). The receptor density of S is significantly higher than that of its neighboring regions.

3.2.3.2. α_2. The α_2 receptors show a distinct regional and laminar distribution pattern in the P7 mouse hippocampal regions (Fig. 3). The receptor densities decrease significantly from the S through CA1 to CA2 and through PreS to PostS (Table 3). Furthermore, the SLM of CA1 and the SM of S both show significantly higher receptor densities, which are visible as a highlighting strip starting at the CA2/CA1 border and abruptly ending at the border of S/PreS. It is noteworthy that the corresponding encoding genes exhibit extremely low expression levels during both the developmental and adult periods.

3.2.4. *Acetylcholine receptors*

The muscarinic M_1, M_2, M_3, and nicotinic $\alpha_4\beta_2$ cholinergic receptors present a relatively homogeneous and low-density distribution pattern in the P7 mouse hippocampal regions (Fig. 4).

3.2.4.1. M_1. The CA1-CA3 regions have comparable M_1 receptor densities (Table 2), which are significantly higher than those of the DG and S (Table 3 and Fig. 4). Regarding the laminar distribution, the SLM in CA3 and SR in CA2 both display higher receptor densities than in other layers. The PostS, especially in the second layer, shows slightly higher receptor density than the PreS. The encoding gene *Chrm1* exhibits a comparable expression level (Fig. 5).

3.2.4.2. M_2. Concerning the M_2 receptor, the DG presents a significantly lower receptor density than its neighboring CA3 region, while the CA1 is significantly lower than the CA2 and S (Table 3 and Fig. 4). The significantly higher receptor densities in CA3 and CA2 than in their respectively adjacent regions DG and CA1 are mainly due to their visibly high receptor density in SP. In addition, the PostS could be clearly separated from the S and PreS mainly by its significantly higher receptor density especially in the second layer. Moreover, a relatively high expression level of the gene *Chrm2* is also observed in the PreS and PostS (Fig. 5).

3.2.4.3. M_3. The M_3 receptor density in the DG is significantly lower than in the CA region, and the S also presents a significantly higher density than the PreS and PostS (Table 3 and Fig. 4). A similar expression pattern is also evident in the expression of the gene *Chrm3* (Fig. 5).

3.2.4.4. Nicotinic $\alpha_4\beta_2$. Concerning the nicotinic $\alpha_4\beta_2$ receptor, the PreS and PostS, containing significantly higher densities, are clearly identified from the S, which also shows a significantly higher density than the CA1 region (Table 3 and Fig. 4). Therefore, the receptor density decreases significantly when moving from the PreS and PostS through S to CA region. Correspondingly, the expression of gene *Chrna4* exhibits a comparable pattern, with high expression levels in the PreS and PostS, followed by a decrease through the S to CA and DG (Fig. 5).

3.2.5. Serotonin receptors

Both 5-HT_{1A} and 5-HT_2 receptors are present at homogenously and very low-density distributions in the P7 mouse hippocampal regions (Fig. 4), and their encoding genes also show extremely low expression levels at P4 (Fig. 5).

3.2.5.1. 5-HT_{1A}. In the case of the 5-HT_{1A} receptor, CA1 and CA2 contain comparable receptor densities, which are significantly higher than in their neighboring regions (Table 3 and Fig. 4). In addition, 5-HT_{1A} receptor densities decrease significantly within the subicular complex, with the highest values detected in PostS and the lowest in S.

3.2.5.2. 5-HT_2. No significant difference was found in 5-HT_2 receptor densities between hippocampal regions in the P7 mouse brain (Fig. 4).

3.2.6. Dopamine receptors

The dopamine D_1 and D_2/D_3 receptors as well as their encoding gens all present low expression levels (Figs. 4 and 5).

3.2.6.1. D_1. For the D_1 receptor, the CA2 shows significantly higher density than its abutting region CA1, and the density decreases significantly through the CA3 to DG (Table 3 and Fig. 4). Furthermore, the S also displays a significantly higher receptor density than its neighboring regions.

3.2.6.2. D_2/D_3. The D_2/D_3 receptor density of the subiculum is significantly higher than the PostS in the P7 mouse hippocampal regions (Table 3 and Fig. 4).

3.2.7. Adenosine receptor

The A_1 receptors show obvious regional and laminar distribution patterns in the P7 mouse hippocampal regions (Fig. 4). The lowest receptor concentration is detected in the DG, which presents significantly lower than in its neighboring CA region (Table 3). The SLM of CA3 and CA2 has the highest receptor density, which distinctly enable identification of the border with the DG and CA1, respectively. In addition, a low-density strip at the level of SP starting at the hilus/CA3 border and abruptly ending at the border between the CA1 and S, is clearly present

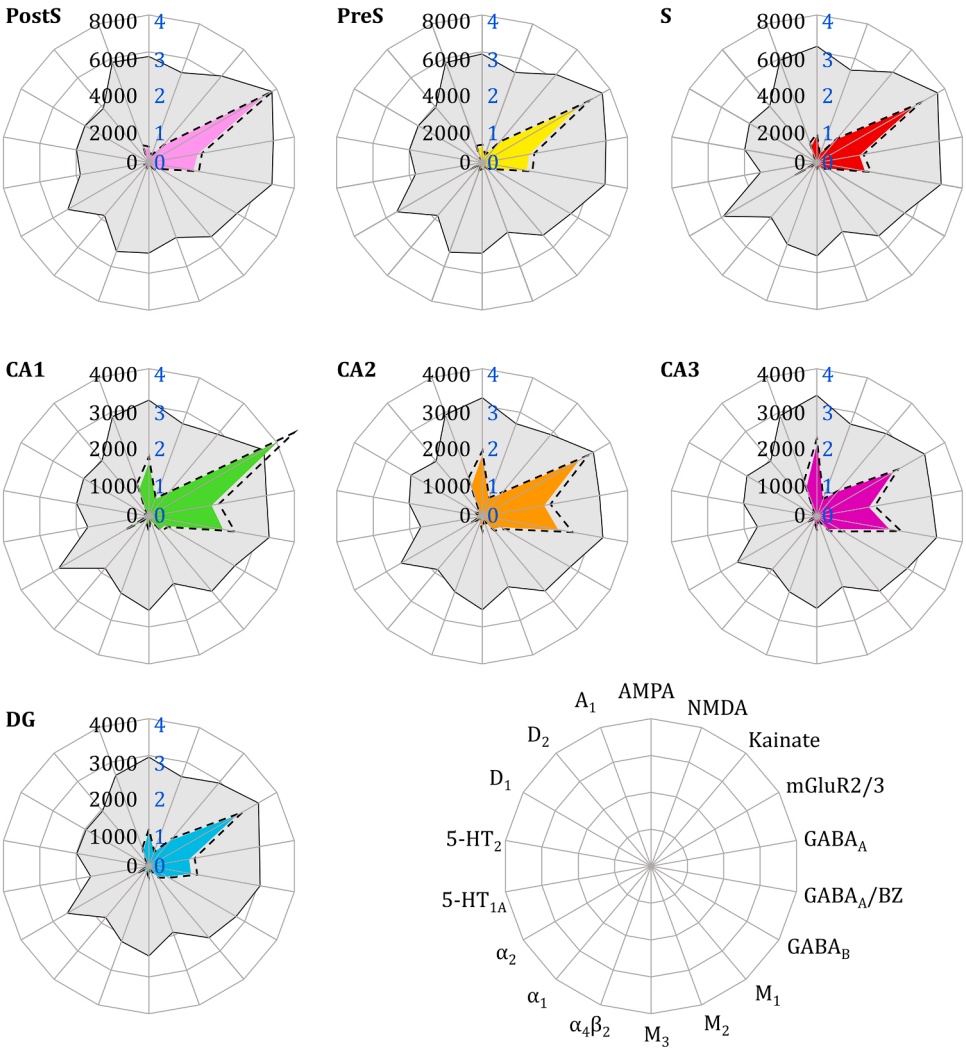

Fig. 7. Receptor fingerprints of P7 mouse hippocampal regions. Each plot depicts the mean absolute density of the 18 analyzed receptors (in fmol/mg protein; colored surface; scale in black font) as well as the corresponding log10 values (gray surface; scale in blue font). The order of receptor types is identical in all fingerprints, which is specified in the polar coordinate plot at the bottom right of the figure. Colored surfaces indicate mean receptor density values, and the corresponding standard deviation is depicted by the dashed lines. The underlying data are provided in Table 2. Note that whereas the log10 scale is the same for all plots (range 0–4), there are differences in the scaling of the absolute densities (in the plots of the CA1-CA3 and DG regions, the scale range is 0–4000 fmol/mg protein; in the subdivisions of the subicular complex, the scale range is 0–8000 fmol/mg protein). Abbreviations: CA1-CA3, sectors 1–3 of *Cornu Ammonis*; DG, dentate gyrus; PostS, postsubiculum; PreS, presubiculum; and S, subiculum. (For interpretation of the references to color in this figure legend, the reader is referred to the web version of this article.)

in the CA region. A relatively homogeneous and significantly higher-density receptor distribution is present in the S than its neighboring regions. The PreS and PostS have lower receptor densities in the second layer, while the PreS contains a higher receptor density in the third layer than that in the PostS.

3.3. Receptor fingerprints and multivariate analyses

Receptor fingerprints of hippocampal regions differ in both size and shape (Fig. 7), where variations in size reflect the differences in absolute receptor densities described for each region, and variations in shape depict the region-specific balance in expression levels of the 18 examined receptor types. The highest absolute density was found for the mGluR2/3 receptor, whereas the 5-HT$_{1A}$ receptor presents the lowest absolute density. The fingerprints of PostS, PreS and S are considerably larger than those of the DG or CA3-CA1 regions, reflecting the higher mGluR2/3 receptor densities found in regions of the subicular complex than in those of the hippocampus proper. In addition to these differences in size, the fingerprints of areas of the subicular complex differ in shape from those of the CA3-CA1 regions and from that of the DG. Within their respective structure (i.e., areas of the subicular complex among each other), the examined areas present similarly shaped fingerprints.

The k-means analyses reveal 4 clusters to be the most stabile configurations for receptor fingerprints of the P7 mouse hippocampal regions, which is consistent with the results of HCA and PCA, respectively (Fig. 8A and B). Specifically, within the hippocampus proper, the CA3-CA1 regions (cluster #1) distinctively separate from the DG region (cluster #2). While within the CA3-CA1 cluster, the CA3 and CA2 are more similar to each other than the CA1. Furthermore, the PreS and PostS regions (cluster #3) could also be distinguished from the S (cluster #4). In the PCA results, the 1st principal component segregates regions of the hippocampus proper from areas of the subicular complex, while the 2nd principal component separates the DG from the CA3-CA1 regions, and the S from the PreS and PostS.

3.4. Different receptor expressions between the P7 and adult brains

The mean receptor densities in the mouse hippocampus at P7 are lower, with considerable variation, compared to the adult brain, with the exception of the α_2 receptor (Fig. 8C). It is worth noting that the

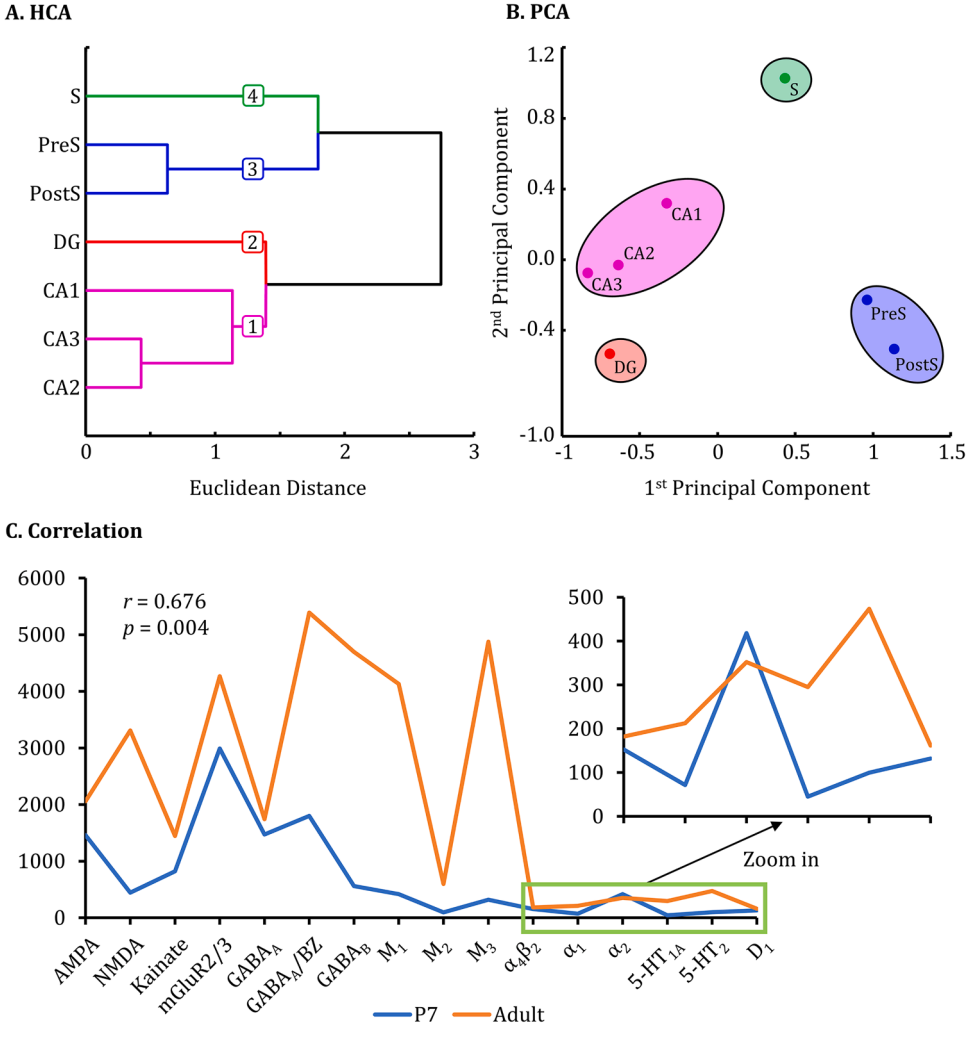

Fig. 8. Multivariate analyses of receptor densities in the P7 mouse hippocampal regions and comparison with the situation in the adult brain. (A) Hierarchical cluster tree (HCA) and (B) principal component analysis (PCA) of the multireceptor fingerprints in P7 mouse hippocampal regions. (C) Analysis of differences in receptor expressions of the mouse hippocampus between the P7 and adult brains. A Spearman correlation was performed using our receptor densities and previously published data (Cremer et al., 2015a, 2015b; Lothmann et al., 2021; Oermann et al., 2005; Zilles et al., 2000) which was obtained from adult individuals of the same mouse strain. The blue line stands for the densities of 16 receptor types distributed in the postnatal mouse hippocampus, while the orange line represents the densities in the adult mouse hippocampus. Abbreviations: CA1-CA3, sectors 1–3 of *Cornu Ammonis*; DG, dentate gyrus; PostS, postsubiculum; PreS, presubiculum; and S, subiculum. (For interpretation of the references to color in this figure legend, the reader is referred to the web version of this article.)

NMDA receptors exhibit the highest density among glutamate receptors in the adult brain, and the opposite holds true in the P7 mouse brain. Interestingly, the relationship between receptor densities in the P7 and adult mouse hippocampus shows a significant positive correlation ($r = 0.676$, $p = 0.004$). Moreover, their nonlinear Granger causality relationship was further demonstrated (mutual information from P7 to adult is 1.065).

4. Discussion

In the present study, we provide a novel and comprehensive description of the cyto- and multireceptor architecture of the hippocampal and subicular regions in the P7 mouse brain, and then compare these findings with the expressions of their encoding genes at P4. This cyto-, gene-, and receptor-multimodal analysis sheds new insights into understanding hippocampal development during the developmental period in the mouse brain. Some of the examined receptors, e.g., mGluR2/3 and $GABA_A$/BZ, are expressed at relatively high densities and present distinctive regional and laminar distribution patterns in this early developmental stage, while other receptors, e.g., 5-HT_{1A} and 5-HT_2, display relatively homogeneous and low-density distributions, and most of their encoding gene expressions exhibit comparable patterns. The region-specific balance expression of multiple receptors in this developing critical period was intuitively visualized as receptor fingerprints, which present differences in size and shape between the different hippocampal regions. Moreover, the hierarchical organization of P7 hippocampal regions as revealed by multivariate cluster analyses based on their receptor fingerprints further confirmed their cytoarchitectonical segregation. Furthermore, for each of the 18 different receptor types, the mean receptor densities (averaged six brains) of P7 hippocampal subregions were transferred to a 3D mouse atlas (Allen Mouse Brain) using the MeshView tool (https://www.nesys.uio.no/MeshView/) for visualization and to facilitate future studies (Fig. 6).

Postnatal day 7 constitutes a developmentally critical period in the mouse brain (Hippenmeyer, 2014). Cortical neurons are initially overabundant due to overexpressed proliferation during early brain development. However, after migrating into their target cortical layer from P7, a large percentage of excess neurons are eliminated through an intrinsically determined program of apoptosis (Dekkers et al., 2013; Denaxa et al., 2018a, 2018b; Southwell et al., 2012). This intrinsically determined cell death plays a critical role in establishing the correct numbers of distinct neuronal populations, as well as in shaping and wiring of the nervous system (Dekkers et al., 2013; Denaxa et al., 2018a). Mirroring these developmental processes and in accordance with previous observations (Paxinos et al., 2020), we found the regions and layers of the P7 mouse hippocampal complex to present a pronouncedly higher cell density than corresponding compartments in the adult brain (Fig. 2). Furthermore, comparison of our results with previously published receptor autoradiographic data on the receptor density and distribution patterns in the adult mouse hippocampal formation (Cremer et al., 2011, 2015a, 2015b; Lothmann et al., 2021; Oermann et al., 2005; Vogt et al., 2013) revealed that these cytoarchitectonic differences are also accompanied by differences in receptor architecture. Although the mean receptor densities in the P7 mouse hippocampus are generally lower with varying degrees of density compared to the adult brain (Fig. 8C), the significant positive correlation between them suggests that, to a certain degree, the mouse hippocampus in both the P7 and adult periods exhibits a similar balance-distribution pattern of multiple receptors, which may imply intrinsic control of cortical development (O'Leary et al., 2007, 2013; Xu et al., 2021). Moreover, the result of Granger causality analysis suggests that the expressions of multiple receptors during the developmental stage may influence their adult expressions, thereby affecting brain function.

Glutamate and GABA are major excitatory and inhibitory neurotransmitters in the mature brain, respectively, and play critical roles in neuronal communication and synaptic plasticity (Collingridge et al., 2004; Groc and Choquet, 2020; Luján et al., 2005). More importantly, the precise temporo-spatial expression and organization of their corresponding receptors are key modulatory factors involved in various stages of normal brain development, such as neuronal proliferation, migration, differentiation, synapse formation and circuit refinement and maturation (Luján et al., 2005). It is worth noting that GABA actions are excitatory during the embryonic stages and the first week of the postnatal period, and this plays a vital role in regulating the cortical development by depolarizing the developing neurons in the immature cortical network (Herlenius and Lagercrantz, 2004; Wang and Kriegstein, 2009). Interestingly, at P7, the NMDA and $GABA_B$ receptors are characterized by relatively homogeneous and low-density distributions in the P7 mouse hippocampal regions (Fig. 3), while they exhibit high receptor densities with distinct regional and laminar distribution patterns in the adult brain (Cremer et al., 2015a, 2015b; Lothmann et al., 2021; Oermann et al., 2005). In contrast, AMPA, Kainate, and $GABA_A$ receptors, and the $GABA_A$/BZ binding sites already exhibit a high-density and distinct heterogeneous regional and laminar distribution at P7 (Fig. 3), but the densities of these receptors are generally lower in the DG at P7 than in adult animals (Cremer et al., 2015a, 2015b; Lothmann et al., 2021; Oermann et al., 2005), which may be associated with its protracted developmental timeline than that of other cortical regions (Esther et al., 2013; Parisot et al., 2017). Moreover, this feature was further confirmed by their gene expression patterns, which present lower expression levels in the DG regions compared to the other regions (Fig. 5). Furthermore, the typically high kainate receptor density in the lucidum layer in the CA3 of adult mice (Cremer et al., 2015a,2015b; Lothmann et al., 2021; Oermann et al., 2005) is not yet present at P7 (Fig. 3). This is not surprising, since the thorny excrescences typical of the mossy fiber terminals do not form from the proximal portion of the pyramidal cell dendrites until postnatal day 9 (Amaral and Dent, 1981). These specific receptor expression patterns during this developing period are in line with their corresponding gene expression levels (Luján et al., 2005). The gene expressions of the main subunits or subtypes of the AMPA, Kainate, mGluR2/3, $GABA_A$ ($GABA_A$/BZ) and $GABA_B$ receptors are already present at comparable patterns in the early postnatal mouse brain (Fig. 5). For NMDA receptors, which were present at relatively low densities throughout the P7 hippocampal complex, the main encoding genes *Grin1* and *Grin2b* already exhibit high expression levels; however, *Grin2a* displays an extremely low expression level (Fig. 5). This asynchronous gene expression pattern may result in the low receptor distributions during this period.

The expressions of receptors for noradrenaline, acetylcholine, serotonin, and dopamine present relatively homogenous and low-density distributions in the P7 mouse hippocampal regions, with the exception of the adrenergic α_2 receptor (Figs. 3 and 4), accompanied by relatively low expression levels of their encoding genes (Fig. 5). However, the adult mouse hippocampus presents high densities and distinct regional and laminar distribution patterns of the M_1, M_3, 5-HT_{1A}, and D_1 receptors when compared with the P7 mouse brain (Cremer et al., 2015a, 2015b; Lothmann et al., 2021). Although M_3, $\alpha_4\beta_2$, α_1, and 5-HT_2 receptors are also homogeneously distributed throughout the adult hippocampus (Cremer et al., 2015a, 2015b; Lothmann et al., 2021), their densities are higher than those seen at P7. Corresponding to the expression levels of these receptors at this early developmental period, the respective neurotransmitters also typically exhibit relatively low levels in the rat hippocampus during early development (Herlenius and Lagercrantz, 2004). For the noradrenaline receptors, the α_1 receptors present relatively low densities in the P7 mouse brain (Fig. 3), which has also been demonstrated in the rat hippocampus by Hartley and Seeman (1983). Moreover, previous studies have reported relatively low α_2 receptor expression levels in the rat hippocampus during the early postnatal period (Hartley and Seeman, 1983; Winzer-Serhan et al., 1996a, b). Furthermore, using membranes from rat brains (excluding the cerebellum), Morris et al. (1980) found that both α_1 and α_2 receptors also exhibit low expression levels during the early postnatal period, and

display a concurrent developmental trend over time (first increasing and then regressing slightly to adult level). However, the α_2 receptors, bound by [^{3}H]-RX821002 ligand in the present study, display distinctively high-density distributions, especially in the SLM of CA1 and the SM of subiculum (Fig. 3). This contradiction may result from the fact that [^{3}H]-RX 821002 possesses a high sensitivity and affinity for α_2 receptors (Clarke and Harris, 2002), approximately 10-fold higher than that of [^{3}H]-idazoxan (Vauquelin et al., 1990), which was used by Winzer--Serhan et al. (1996a). Interestingly, the encoding genes *Adra2a*, *Adra2b*, and *Adra2c* in the mouse brain exhibit extremely low expression levels in both developmental and adult periods; however, the α_2 receptors are already present in high densities with distinct regional and laminal distribution patterns in both the P7 (present study, Fig. 4) and adult mouse brain (Lothmann et al., 2021). These results suggest that a non-covariation differentiation phenomenon between α_2 receptor distributions and corresponding gene expressions is already present in the early developmental period.

Adenosine is an important neuromodulator in the mammalian central nervous system and plays a pivotal role in the brain with its corresponding receptors, e.g., homeostatic regulation of circadian timing (Daval et al., 1991; Herlenius and Lagercrantz, 2004; Hocher, 2010; Jagannath et al., 2021). In the present study, we observed a high density of A_1 receptors with a distinct regional and laminar distribution pattern in the P7 mouse hippocampal complex (Fig. 4), which has also been demonstrated by Daval et al. (1991). They found a quite low and homogeneous receptor distribution pattern at birth, followed by a prominent increase during the first ten postnatal days. This sequential expression of A_1 receptors in the rat hippocampus during brain development is in relation to the time course of maturation of the brain (Daval et al., 1991). These results suggest that adenosine is implicated in early hippocampal development via its A_1 receptor (Herlenius and Lagercrantz, 2004).

It is noteworthy that receptors with low densities during a specific developmental period, as illustrated in Figs. 3 and 4, also contribute to enable normal brain development, because overexpression of these receptors during early hippocampal development can induce various neurodevelopmental dysfunctions, including anxiety, emotion regulation, and spatial learning and memory (Bert et al., 2005; Kusserow et al., 2004). Therefore, normal brain development is intrinsically regulated by the precise spatial and temporal balance expressions of multiple neurotransmitter receptors (Gaspar et al., 2003; Herlenius and Lagercrantz, 2004; Luján et al., 2005; Ojeda and Ávila, 2019). However, previous studies only focused on one or a few neurotransmitter receptors (Daval et al., 1991; Hartley and Seeman, 1983; Morris et al., 1980; Winzer-Serhan et al., 1996a, 1996b), thus a comprehensive characterization of multi-receptor expression during the specific brain development period of P7 is highly relevant, but currently lacking. Hereby, we have comprehensively and systematically characterized the balanced expressions of 18 different receptor types in all regions of the hippocampal complex, visualizing them as receptor fingerprints (Fig. 7) during a critical period of mouse brain development. This provides new insights into a deeper understanding of brain development from the perspective of specific multi-receptor balanced expression. E.g., with the notable exception of the kainate receptor, the densities of all receptors analyzed here are lower in the DG than in its neighboring regions. Moreover, the receptor fingerprints of hippocampal regions in this period align with the organization relationships identified through cytoarchitecture, as demonstrated by the HCA and PCA results (Fig. 8). These results suggest a relationship of interdependence between cyto- and receptor architecture during hippocampal development.

The method used in the present study has the enormous advantage of enabling the detection and absolute quantification of extremely low densities of receptors in their native configuration with a high degree of spatial resolution (Palomero-Gallagher and Zilles, 2018). This spatial resolution allows for measurements in relatively small structures, such as the individual hippocampal layers in the brain of newborn mice (Figs. 3 and 4). The hippocampal circuitry has been very well characterized, providing information on the specific layers targeted by intra- and inter-hippocampal connectivity (Dudek et al., 2016, 2023; Geiller et al., 2017; Zeineh et al., 2017), thus enabling the possibility to make assumptions concerning the functional relevance of layer-specific differences in receptor densities. However, it must be noted that our conclusions are limited by the fact that quantitative *in vitro* receptor autoradiography does not enable identification of the cells expressing these receptors (Palomero-Gallagher and Zilles, 2018), and that the CA and DG regions not only contain pyramidal and granular cells, respectively, but also a myriad of interneurons with specific laminar localizations (Wheeler et al., 2015). The second limitation is that the receptor and gene expression data were obtained from different developmental stages (P7 vs. P4) and sectioning planes (coronal vs. sagittal). Although the functional differentiation of hippocampal cells along different axes may not be very significant during the very early developmental period (Iacono et al., 2017; Lohmann and Kessels, 2014), these differences can influence the outcomes of comparisons to a certain extent and warrant further investigation.

In conclusion, we provide a comprehensive characterization of the cyto-, gene and receptor architecture of the developing mouse hippocampal complex. The specific balance expression of multiple genes and receptors during this developmental period, which differs from the corresponding distribution patterns in the adult brain but have a high correlation between receptor data, suggests the importance of this specific spatial and temporal expression necessary for enabling the normal development of the hippocampal regions. Moreover, the specific expression of multiple receptors is tightly controlled by spatial and temporal intrinsic regulation, and coincides with regional cytoarchitecture, neurotransmitter distributions, and gene expressions. This multiple gene and receptor data offer new insights into their specific expression and suggest further roles in early postnatal hippocampal development, and contribute important molecular data for further interdisciplinary studies.

Funding

This project has received funding from the European Union's Horizon 2020 Research and Innovation Programme under the Specific Grant Agreement 945539 (Human Brain Project SGA3), and from the Helmholtz Association's Initiative and Networking Fund through the Helmholtz International BigBrain Analytics and Learning Laboratory (HIBALL) under the Helmholtz International Lab grant agreement InterLabs-0015.

CRediT authorship contribution statement

Nicola Palomero-Gallagher: Writing – review & editing, Writing – original draft, Supervision, Resources, Project administration, Funding acquisition, Data curation, Conceptualization. **Menno P. Witter:** Writing – review & editing, Writing – original draft, Conceptualization. **Ling Zhao:** Writing – review & editing, Writing – original draft, Visualization, Software, Methodology, Investigation, Formal analysis, Data curation.

Declaration of Competing Interest

Authors declare that they have no competing interests.

Acknowledgements

This article is dedicated to Professor Dr. med. Dr. h.c. Karl Zilles, deceased the 26th of April 2020, who was fully involved in the planning of the project, and we are greatly indebted to his neuroscientific legacy. We also extend our gratitude to Dr. Kevin Jones and Dr. Shen-Ju Chou for kindly providing the mouse brains.

Appendix A. Supporting information

Supplementary data associated with this article can be found in the online version at doi:10.1016/j.pneurobio.2024.102704.

Data availability

Data will be made available on request.

References

Acsády, L., Káli, S., 2007. Models, structure, function: the transformation of cortical signals in the dentate gyrus. In: Scharfman, H.E. (Ed.), Progress in Brain Research. Elsevier, pp. 577–599.

Amaral, D.G., Dent, J.A., 1981. Development of the mossy fibers of the dentate gyrus: I. A light and electron microscopic study of the mossy fibers and their expansions. J. Comp. Neurol. 195, 51–86.

Baayen, R.H., Davidson, D.J., Bates, D.M., 2008. Mixed-effects modeling with crossed random effects for subjects and items. J. Mem. Lang. 59, 390–412.

Barr, D.J., Levy, R., Scheepers, C., Tily, H.J., 2013. Random effects structure for confirmatory hypothesis testing: keep it maximal. J. Mem. Lang. 68, 255–278.

Bates, D., Kliegl, R., Vasishth, S., Baayen, H., 2015. Parsimonious mixed Models. arXiv preprint arXiv:.04967.

Benjamini, Y., Hochberg, Y., 1995. Controlling the false discovery rate: a practical and powerful approach to multiple testing. J. R. Stat. Soc. Ser. B (Methodol. 57, 289–300.

Berger, T., Lee, H., Young, A.H., Aarsland, D., Thuret, S., 2020. Adult hippocampal neurogenesis in major depressive disorder and Alzheimer's disease. Trends Mol. Med. 26, 803–818.

Bert, B., Dere, E., Wilhelmi, N., Kusserow, H., Theuring, F., Huston, J.P., Fink, H., 2005. Transient overexpression of the 5-HT1A receptor impairs water-maze but not hole-board performance. Neurobiol. Learn Mem. 84, 57–68.

Bird, C.M., Burgess, N., 2008. The hippocampus and memory: insights from spatial processing. Nat. Rev. Neurosci. 9, 182–194.

Borges, K., Myers, S.J., Zhang, S., Dingledine, R., 2003. Activity of the rat GluR4 promoter in transfected cortical neurons and glia. J. Neurochem. 86, 1162–1173.

Cameron, H.A., Hazel, T.G., McKay, R.D.G., 1998. Regulation of neurogenesis by growth factors and neurotransmitters. J. Neurobiol. 36, 287–306.

Cameron, H.A., McKay, R.D.G., 2001. Adult neurogenesis produces a large pool of new granule cells in the dentate gyrus. J. Comp. Neurol. 435, 406–417.

Chandra, D., Halonen, L.M., Linden, A.M., Procaccini, C., Hellsten, K., Homanics, G.E., Korpi, E.R., 2010. Prototypic GABA(A) receptor agonist muscimol acts preferentially through forebrain high-affinity binding sites. Neuropsychopharmacology 35, 999–1007.

Chiang, S.-Y., Wu, H.-C., Lin, S.-Y., Chen, H.-Y., Wang, C.-F., Yeh, N.-H., Shih, J.-H., Huang, Y.-S., Kuo, H.-C., Chou, S.-J., Chen, R.-H., 2021. Usp11 controls cortical neurogenesis and neuronal migration through Sox11 stabilization. Sci. Adv. 7, eabc6093.

Chuang, S.-H., Reddy, D.S., 2018. Genetic and molecular regulation of extrasynaptic gaba-a receptors in the brain: therapeutic insights for epilepsy. J. Pharmacol. Exp. Ther. 364, 180.

Clarke, R.W., Harris, J., 2002. RX 821002 as a tool for physiological investigation of α2-adrenoceptors. CNS Drug Rev. 8, 177–192.

Collingridge, G.L., Isaac, J.T., Wang, Y.T., 2004. Receptor trafficking and synaptic plasticity. Nat. Rev. Neurosci. 5, 952–962.

Cremer, C.M., Lübke, J.H.R., Palomero-Gallagher, N., Zilles, K., 2011. Laminar distribution of neurotransmitter receptors in different reeler mouse brain regions. Brain Struct. Funct. 216, 201–218.

Cremer, J.N., Amunts, K., Graw, J., Piel, M., Rösch, F., Zilles, K., 2015a. Neurotransmitter receptor density changes in Pitx3ak mice – a model relevant to Parkinson's disease. Neuroscience 285, 11–23.

Cremer, J.N., Amunts, K., Schleicher, A., Palomero-Gallagher, N., Piel, M., Rösch, F., Zilles, K., 2015b. Changes in the expression of neurotransmitter receptors in Parkin and DJ-1 knockout mice – A quantitative multireceptor study. Neuroscience 311, 539–551.

Crews, F., He, J., Hodge, C., 2007. Adolescent cortical development: a critical period of vulnerability for addiction. Pharmacol. Biochem. Behav. 86, 189–199.

Daval, J.L., Werck, M.C., Nehlig, A., de Vasconcelos, A.P., 1991. Quantitative autoradiographic study of the postnatal development of adenosine A1 receptors and their coupling to G proteins in the rat brain. Neuroscience 40, 841–851.

Debski, K.J., Ceglia, N., Ghestem, A., Ivanov, A.I., Brancati, G.E., Broer, S., Bot, A.M., Muller, J.A., Schoch, S., Becker, A., Loscher, W., Guye, M., Sassone-Corsi, P., Lukasiuk, K., Baldi, P., Bernard, C., 2020. The circadian dynamics of the hippocampal transcriptome and proteome is altered in experimental temporal lobe epilepsy. Sci. Adv. 6, eaat5979.

Dekkers, M.P.J., Nikoletopoulou, V., Barde, Y.-A., 2013. Death of developing neurons: new insights and implications for connectivity. J. Cell Biol. 203, 385–393.

Denaxa, M., Neves, G., Burrone, J., Pachnis, V., 2018a. Homeostatic regulation of interneuron apoptosis during cortical development. J. Exp. Neurosci. 12, 1179069518784277.

Denaxa, M., Neves, G., Rabinowitz, A., Kemlo, S., Liodis, P., Burrone, J., Pachnis, V., 2018b. Modulation of apoptosis controls inhibitory interneuron number in the cortex. Cell Rep. 22, 1710–1721.

Dong, H.W., 2008. The Allen Reference Atlas: a Digital Color Brain Atlas of The C57Bl/6J Male Mouse. John Wiley & Sons Inc, Hoboken, NJ, US.

Dudek, S.M., Alexander, G.M., Farris, S., 2016. Rediscovering area CA2: unique properties and functions. Nat. Rev. Neurosci. 17, 89–102.

Dudek, S.M., Alexander, G.M., Farris, S., 2023. Introduction to the special issue on: a new view of hippocampal area CA2. Hippocampus 33, 127–132.

Ecker, A., Bagi, B., Vértes, E., Steinbach-Németh, O., Karlócai, M.R., Papp, O.I., Miklós, I., Hájos, N., Freund, T.F., Gulyás, A.I., Káli, S., 2022. Hippocampal sharp wave-ripples and the associated sequence replay emerge from structured synaptic interactions in a network model of area CA3. eLife 11, e71850.

Esther, P.Y., Christopher, G.D., Shanti, F.F., Mary, E.P., Cuiyong, Y., Hajime, T., Douglas, A.C., 2013. Protracted postnatal development of sparse, specific dentate granule cell activation in the mouse hippocampus. J. Neurosci. 33, 2947.

Feng, J., Hsu, W.-H., Patterson, D., Tseng, C.-S., Hsing, H.-W., Zhuang, Z.-H., Huang, Y.-T., Faedo, A., Rubenstein, J.L., Touboul, J., Chou, S.-J., 2021. COUP-TFI specifies the medial entorhinal cortex identity and induces differential cell adhesion to determine the integrity of its boundary with neocortex. Sci. Adv. 7, eabf6808.

Gallyas, F., 1979. Silver staining of myelin by means of physical development. Neurol. Res. 1, 203–209.

Gaspar, P., Cases, O., Maroteaux, L., 2003. The developmental role of serotonin: news from mouse molecular genetics. Nat. Rev. Neurosci. 4, 1002–1012.

Geiller, T., Royer, S., Choi, J.S., 2017. Segregated cell populations enable distinct parallel encoding within the radial axis of the CA1 pyramidal layer. Exp. Neurobiol. 26, 1–10.

Geyer, S., Matelli, M., Luppino, G., Schleicher, A., Jansen, Y., Palomero-Gallagher, N., Zilles, K., 1998. Receptor autoradiographic mapping of the mesial motor and premotor cortex of the macaque monkey. J. Comp. Neurol. 397, 231–250.

Groc, L., Choquet, D., 2020. Linking glutamate receptor movements and synapse function. Science 368, eaay4631.

Hartley, E.J., Seeman, P., 1983. Development of receptors for dopamine and noradrenaline in rat brain. Eur. J. Pharmacol. 91, 391–397.

Heiss, W.-D., Herholz, K., 2006. Brain Receptor Imaging. J. Nucl. Med. 47, 302.

Herlenius, E., Lagercrantz, H., 2004. Development of neurotransmitter systems during critical periods. Exp. Neurol. 190, 8–21.

Hippenmeyer, S., 2014. Molecular pathways controlling the sequential steps of cortical projection neuron migration. In: Nguyen, L., Hippenmeyer, S. (Eds.), Cellular and Molecular Control of Neuronal Migration. Springer Netherlands, Dordrecht, pp. 1–24.

Hocher, B., 2010. Adenosine A1 receptor antagonists in clinical research and development. Kidney Int. 78, 438–445.

Iacono, G., Benevento, M., Dubos, A., Herault, Y., van Bokhoven, H., Nadif Kasri, N., Stunnenberg, H.G., 2017. Integrated transcriptional analysis unveils the dynamics of cellular differentiation in the developing mouse hippocampus. Sci. Rep. 7, 18073.

Jagannath, A., Varga, N., Dallmann, R., Rando, G., Gosselin, P., Ebrahimjee, F., Taylor, L., Mosneagu, D., Stefaniak, J., Walsh, S., Palumaa, T., Di Pretoro, S., Sanghani, H., Wakaf, Z., Churchill, G.C., Galione, A., Peirson, S.N., Boison, D., Brown, S.A., Foster, R.G., Vasudevan, S.R., 2021. Adenosine integrates light and sleep signalling for the regulation of circadian timing in mice. Nat. Commun. 12, 2113.

Khan, A.F., Adewale, Q., Baumeister, T.R., Carbonell, F., Zilles, K., Palomero-Gallagher, N., Iturria-Medina, Y., Alzheimer's Disease Neuroimaging, I., 2021. Personalized brain models identify neurotransmitter receptor changes in Alzheimer's disease. Brain, awab375.

Kraskov, A., Stögbauer, H., Grassberger, P., 2004. Estimating mutual information. Phys. Rev. E 69, 066138.

Kusserow, H., Davies, B., Hörtnagl, H., Voigt, I., Stroh, T., Bert, B., Deng, D.R., Fink, H., Veh, R.W., Theuring, F., 2004. Reduced anxiety-related behaviour in transgenic mice overexpressing serotonin1A receptors. Mol. Brain Res. 129, 104–116.

Kuznetsova, A., Brockhoff, P.B., Christensen, R.H.B., 2017. lmerTest package: tests in linear mixed effects models. J. Stat. Softw. 82, 26.

Lau, C.G., Zukin, R.S., 2007. NMDA receptor trafficking in synaptic plasticity and neuropsychiatric disorders. Nat. Rev. Neurosci. 8, 413–426.

Levitt, P., Harvey, J.A., Friedman, E., Simansky, K., Murphy, E.H., 1997. New evidence for neurotransmitter influences on brain development. Trends Neurosci. 20, 269–274.

Lohmann, C., Kessels, H.W., 2014. The developmental stages of synaptic plasticity. J. Physiol. 592, 13–31.

Lothmann, K., Deitersen, J., Zilles, K., Amunts, K., Herold, C., 2021. New boundaries and dissociation of the mouse hippocampus along the dorsal-ventral axis based on glutamatergic, GABAergic and catecholaminergic receptor densities. Hippocampus 31, 56–78.

Luján, R., Shigemoto, R., López-Bendito, G., 2005. Glutamate and GABA receptor signalling in the developing brain. Neuroscience 130, 567–580.

McGowan, E., Eriksen, J., Hutton, M., 2006. A decade of modeling Alzheimer's disease in transgenic mice. Trends Genet. 22, 281–289.

Morris, M.J., Dausse, J.-P., Devynck, M.-A., Meyer, P., 1980. Ontogeny of α1andα2-adrenoceptors in rat brain. Brain Res. 190, 268–271.

Nagode, D.A., Meng, X., Winkowski, D.E., Smith, E., Khan-Tareen, H., Kareddy, V., Kao, J.P.Y., Kanold, P.O., 2017. Abnormal development of the earliest cortical circuits in a mouse model of autism spectrum disorder. Cell Rep. 18, 1100–1108.

Nichols, T.E., Holmes, A.P., 2002. Nonparametric permutation tests for functional neuroimaging: a primer with examples. Hum. Brain Mapp. 15, 1–25.

O'Leary, D., Stocker, A., Zembrzycki, A., 2013. Area patterning of the mammalian cortex. Patterning and Cell Type Specification in the Developing Cns and Pns 61–85.

O'Leary, D.D.M., Chou, S.-J., Sahara, S., 2007. Area patterning of the mammalian cortex. Neuron 56, 252–269.

Oermann, E., Warskulat, U., Heller-Stilb, B., Häussinger, D., Zilles, K., 2005. Taurine-transporter gene knockout-induced changes in GABAA, kainate and AMPA but not NMDA receptor binding in mouse brain. Anat. Embryol. 210, 363–372.
Ojeda, J., Ávila, A., 2019. Early actions of neurotransmitters during cortex development and maturation of reprogrammed neurons. Front. Synaptic Neurosci. 11.
Palomero-Gallagher, N., Zilles, K., 2018. Cyto- and receptor architectonic mapping of the human brain. In: Huitinga, I., Webster, M.J. (Eds.), Handb Clin Neurol. Elsevier, pp. 355–387.
Paoletti, P., Bellone, C., Zhou, Q., 2013. NMDA receptor subunit diversity: impact on receptor properties, synaptic plasticity and disease. Nat. Rev. Neurosci. 14, 383–400.
Parisot, J., Flore, G., Bertacchi, M., Studer, M., 2017. COUP-TFI mitotically regulates production and migration of dentate granule cells and modulates hippocampal Cxcr4 expression. Development 144, 2045–2058.
Paxinos, G., Halliday, G., Watson, C., Kassem, M., 2020. Atlas of the Developing Mouse Brain. Academic Press.
Represa, A., Robain, O., Tremblay, E., Ben-Ari, Y., 1989. Hippocampal plasticity in childhood epilepsy. Neurosci. Lett. 99, 351–355.
Rousseeuw, P.J., 1987. Silhouettes: a graphical aid to the interpretation and validation of cluster analysis. J. Comput. Appl. Math. 20, 53–65.
Simonnet, J., Nassar, M., Stella, F., Cohen, I., Mathon, B., Boccara, C.N., Miles, R., Fricker, D., 2017. Activity dependent feedback inhibition may maintain head direction signals in mouse presubiculum. Nat. Commun. 8, 16032.
Snyder, J.S., 2019. Recalibrating the relevance of adult neurogenesis. Trends Neurosci. 42, 164–178.
Snyder, J.S., Soumier, A., Brewer, M., Pickel, J., Cameron, H.A., 2011. Adult hippocampal neurogenesis buffers stress responses and depressive behaviour. Nature 476, 458–461.
Southwell, D.G., Paredes, M.F., Galvao, R.P., Jones, D.L., Froemke, R.C., Sebe, J.Y., Alfaro-Cervello, C., Tang, Y., Garcia-Verdugo, J.M., Rubenstein, J.L., Baraban, S.C., Alvarez-Buylla, A., 2012. Intrinsically determined cell death of developing cortical interneurons. Nature 491, 109–113.
van Strien, N.M., Cappaert, N.L.M., Witter, M.P., 2009. The anatomy of memory: an interactive overview of the parahippocampal–hippocampal network. Nat. Rev. Neurosci. 10, 272–282.
Vauquelin, G., De Vos, H., De Backer, J.-P., Ebinger, G., 1990. Identification of α2 adrenergic receptors in human frontal cortex membranes by binding of [3H]RX 821002, the 2-methoxy analog of [3H]idazoxan. Neurochem. Int. 17, 537–546.
Verdurand, M., Fillman, S.G., Shannon Weickert, C., Zavitsanou, K., 2013. Increases in [3H] muscimol and [3H] flumazenil binding in the dorsolateral prefrontal cortex in schizophrenia are linked to α4 and γ2S mRNA levels respectively. PLoS One 8, e52724.
Vogt, B.A., Hof, P.R., Zilles, K., Vogt, L.J., Herold, C., Palomero-Gallagher, N., 2013. Cingulate area 32 homologies in mouse, rat, macaque and human: cytoarchitecture and receptor architecture. J. Comp. Neurol. 521, 4189–4204.
Wang, D.D., Kriegstein, A.R., 2009. Defining the role of GABA in cortical development. J. Physiol. 587, 1873–1879.
Wheeler, D.W., White, C.M., Rees, C.L., Komendantov, A.O., Hamilton, D.J., Ascoli, G.A., 2015. Hippocampome.org: a knowledge base of neuron types in the rodent hippocampus. Elife 4.
Winzer-Serhan, U.H., Raymon, H.K., Broide, R.S., Chen, Y., Leslie, F.M., 1996b. Expression of α2 adrenoceptors during rat brain development—II. α2C messenger RNA expression and [3H]rauwolscine binding. Neuroscience 76, 261–272.
Winzer-Serhan, U.H., Raymon, H.K., Broide, R.S., Chen, Y., Leslie, F.M., 1996a. Expression of α2 adrenoceptors during rat brain development—I. α2A messenger RNA expression. Neuroscience 76, 241–260.
Witter, M., 2012. Hippocampus. In: Watson, C., Paxinos, G., Puelles, L. (Eds.), The Mouse Nervous System. Academic Press, San Diego, pp. 112–139.
Xu, L., Zheng, Y., Li, X., Wang, A., Huo, D., Li, Q., Wang, S., Luo, Z., Liu, Y., Xu, F., Wu, X., Wu, M., Zhou, Y., 2021. Abnormal neocortex arealization and Sotos-like syndrome–associated behavior in Setd2 mutant mice. Sci. Adv. 7, eaba1180.
Zeineh, M.M., Palomero-Gallagher, N., Axer, M., Gräβel, D., Goubran, M., Wree, A., Woods, R., Amunts, K., Zilles, K., 2017. Direct visualization and mapping of the spatial course of fiber tracts at microscopic resolution in the human hippocampus. Cereb. Cortex 27, 1779–1794.
Zhao, L., Mühleisen, T.W., Pelzer, D.I., Burger, B., Beins, E.C., Forstner, A.J., Herms, S., Hoffmann, P., Amunts, K., Palomero-Gallagher, N., Cichon, S., 2023. Relationships between neurotransmitter receptor densities and expression levels of their corresponding genes in the human hippocampus. NeuroImage 273, 120095.
Zhong, S., Ding, W., Sun, L., Lu, Y., Dong, H., Fan, X., Liu, Z., Chen, R., Zhang, S., Ma, Q., Tang, F., Wu, Q., Wang, X., 2020. Decoding the development of the human hippocampus. Nature 577, 531–536.
Zhou, Y., Su, Y., Li, S., Kennedy, B.C., Zhang, D.Y., Bond, A.M., Sun, Y., Jacob, F., Lu, L., Hu, P., Viaene, A.N., Helbig, I., Kessler, S.K., Lucas, T., Salinas, R.D., Gu, X., Chen, H. I., Wu, H., Kleinman, J.E., Hyde, T.M., Nauen, D.W., Weinberger, D.R., Ming, G.-l, Song, H., 2022. Molecular landscapes of human hippocampal immature neurons across lifespan. Nature 607, 527–533.
Zilles, K., Schleicher, A., Palomero-Gallagher, N., Amunts, K., 2002. Quantitative analysis of cyto- and receptor architecture of the human brain. In: Toga, A.W., Mazziotta, J.C. (Eds.), Brain Mapping: The Methods, second ed. Academic Press, San Diego, pp. 573–602.
Zilles, K., Wu, J., Crusio, W.E., Schwegler, H., 2000. Water maze and radial maze learning and the density of binding sites of glutamate, GABA, and serotonin receptors in the hippocampus of inbred mouse strains. Hippocampus 10, 213–225.